Analytical Models for Reinforced Concrete Columns Retrofitted with Fiber-Reinforced Polymer Composites

A Thesis

Presented in Partial Fulfillment of the Requirements for

Graduation with Distinction with the Degree Bachelor of Science

in the Civil Engineering Department of the

College of Engineering of The Ohio State University

By

Jason Donald Ross

The Ohio State University

2007

Undergraduate Honors Examination Committee:

Dr. Halil Sezen, Advisor

Dr. Patrick Fox

Approved by:

Advisor

Civil Engineering Undergraduate Honors Program

ABSTRACT

Traditional rebar reinforcement methods in concrete columns have been accepted for many years as the common practice among designers and contractors. There has been a tremendous amount of research completed and designers are capable of predicting the future performance of the columns. More recently, retrofit methods have been used on aging concrete columns. This includes adding an additional layer of concrete or composite material around the existing column to slow the deterioration and to increase the concrete confinement. Current models exist in the use of a combination of a rebar cage and concrete as the retrofit method.

Fiber-reinforced polymer (FRP) wraps are fast becoming a new form of technology to replace traditional rebar retrofit technology. The fiber-reinforced polymer wraps are a composite material that can be attached to the existing concrete column using an epoxy resin. The wrap increases the concrete confinement of the column and provides support for the concrete dilation in the column. However, FRP wraps are not heavily used in structural applications because there is not an accepted model that has been proven to accurately predict future strength characteristics of the confined concrete column.

The focus of this research project is to use the results of an already completed test of concrete columns confined by FRP wraps, and compare the resulting stress-strain curves to the commonly proposed modeling technology available. FRP modeling is still relatively new and there is not a widely accepted model.

The purpose of this research project is to determine how accurately the proposed FRP models predict the strength of the tested columns. There are many different models that have been proposed, but the key to the future of FRP retrofitting is to create a widely accepted, reliable model that engineers can use in design. It is important to normalize the design process of FRP retrofitted columns in order to better use the technology in the future.

TABLE OF CONTENTS

LIST OF FIGURES

LIST OF TABLES

CHAPTER 1

INTRODUCTION & BACKGROUND INFORMATION

1.1 Introduction

Fiber-reinforced polymer, FRP is a composite material containing fibers in a polymer matrix. The FRP is typically applied with an epoxy resin. The epoxy resin is used to combine the fibers and connect the wrap with the structural member. The reinforcement system works together as a cohesive unit, and if one part of the fiber is weak, the entire system will have a brittle failure as a result. The advantages of the FRP wrap are many. These include increased concrete confinement, corrosion resistance, high specific strength, and durability (Bischoff 2003). While FRP can be used to strengthen many different structural members, the focus of this paper will be its application for retrofitting columns. The search to find a widely accepted model for the FRP reinforcement system in columns is on-going and will be closely summarized and examined in this research study.

1.2 Methods of Reinforcement

Throughout the years, research in structural engineering has created many different reinforcement and retrofit/strengthening methods for structural members. The most popular of these being reinforcing bar, or rebar cages. However, some of the other practices include fiber-reinforced polymer (FRP), concrete-filled tubes (CFT), and welded wire fabric (WWF). All methods have their advantages and disadvantages. In this research, the focus will be primarily on fiber-reinforced polymer as a retrofit method and the traditional rebar cages as reinforcement.

1.2.1 Traditional Rebar Reinforcement System

The most widely accepted and used method for reinforcement in structural applications is the steel rebar cage. Concrete and steel work very well together in a structural application. The design of columns is centered on having the concrete to resist the compressive forces because concrete is strong in compression. Furthermore, the steel is present in the column to resist any tensile forces, as steel is strong in tension, as well as in compression. The steel is designed as a cage to surround the concrete, while concrete is poured inside and outside this cage to the limits of the formwork. The inner concrete is intended to carry most of the applied compressive load, while the outside or "cover" concrete protects the steel from weather, fire, and corrosion. The steel is placed in two directions, longitudinal and transverse. The longitudinal steel helps to carry the tension loads as well as the compressive load. The transverse steel wraps around the longitudinal steel to help in the confinement of the concrete and resist shear forces. Figure 1.1 displays how the steel can mesh very well as a complete reinforcement system.

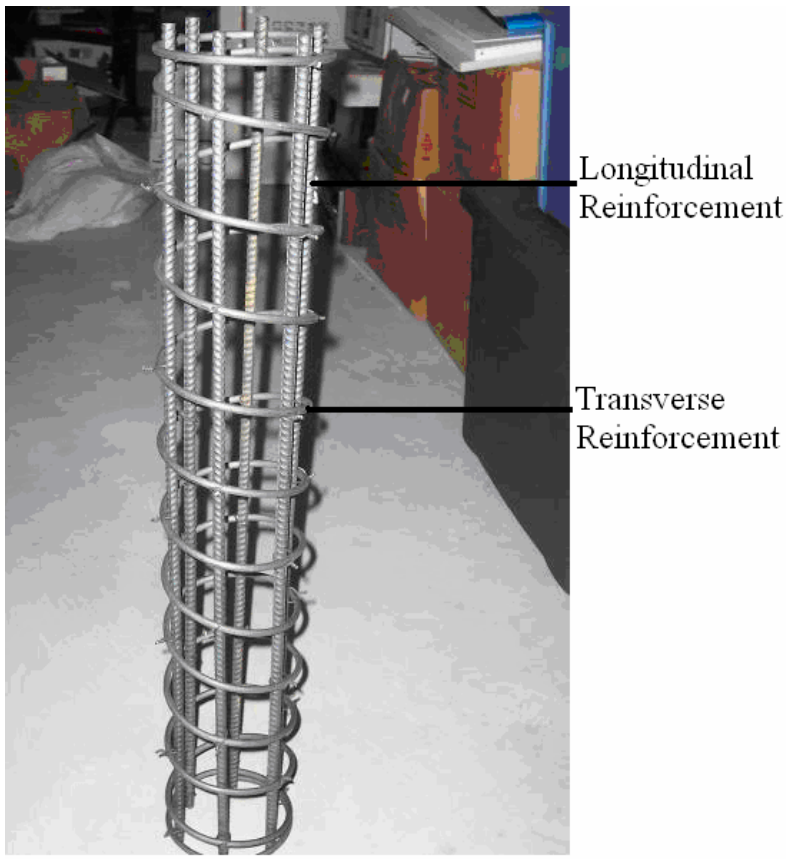

Figure 1.1 – Setup of Rebar Cages (Miller 2006).

1.2.2 Fiber-reinforced Polymer (FRP) System

Fiber-reinforced polymer is a composite material that consists of a polymer matrix with fiber reinforcement. Glass and Carbon are common fibers while the polymer is typically an epoxy resin. The polymer is placed on the concrete surface, then the FRP is wrapped around the column or beam. In wet-application, fibers are soaked in wet resin or polymer before FRP application. The polymer helps to connect the fibers of the wrap together while also making a strong connection with the surface of the concrete.

An FRP system wrapped around a column provides passive reinforcement to the column. As the concrete member is loaded axially, the FRP reinforcement system provides little or no effect on strength increase to the confined concrete initially. However, once the concrete dilates and begins to crack and weaken, the FRP reinforcement provides confinement for the concrete. The stress-strain diagram presented in Figure 1.2 will continue on a second linear path before reaching a brittle failure at a much higher axial stress and axial strain than the initial unretrofitted failure point. The main advantage of the FRP system is the amount of confinement that it provides. The enveloping wrap or tube provides more confinement than a longitudinal or spirally wrapped steel rebar.

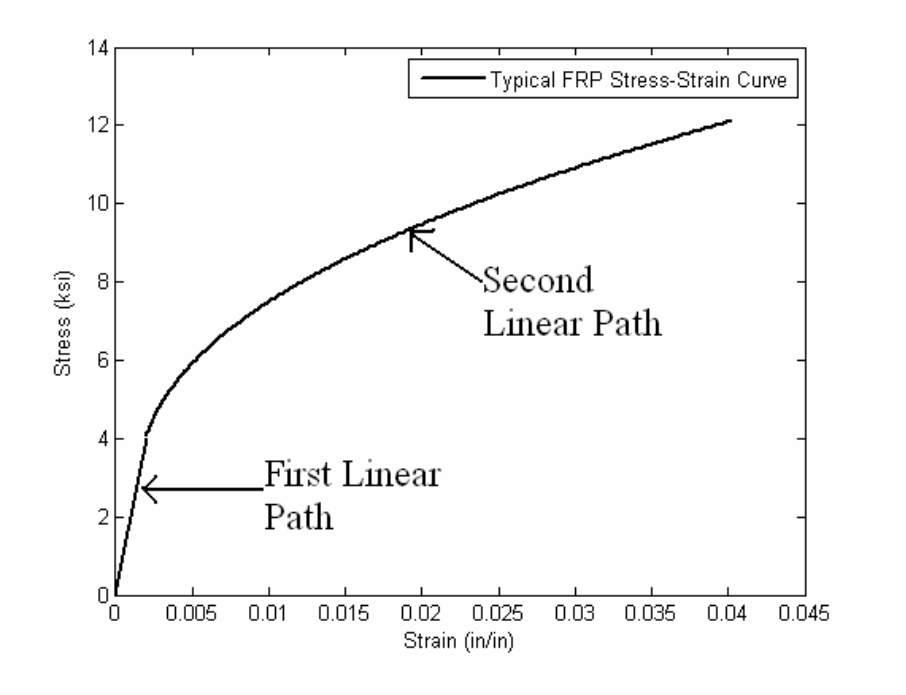

Figure 1.2 – Typical FRP Stress-Strain Diagram

1.3 Comparison of Steel Rebar and FRP Systems

1.3.1 Production Comparison

The production of traditional rebar is widespread and defined due to its high usage. The common sizes and widely accepted designs make the production of traditional rebar cost-effective. The production of FRP materials is not as common. However, with the acceptance of FRP reinforcement as a viable option in construction, the manufacturing time would greatly reduce. The FRP wraps could be mass produced into rolls of many different sizes depending on the application. The larger sizes would be best, to allow the least amount of joints and imperfections in construction as possible. The prefabricated FRP tubes would require the largest production time, but still could be constructed in common sizes. The upside of an FRP tube is that it lessens the chance for construction mistakes to occur. The main dissenting fact about the FRP system is that the cost of fiber and epoxy resin is high (Nystrom et al. 2003).

1.3.2 Time of Construction

The construction time for the two systems is a determinant of which type of reinforcement is better suited for the project. The more time spent constructing the reinforcement system, the higher the cost of the overall project. Traditional rebar reinforcement has been the long accepted practice for initial reinforcement, but not as a retrofit method. Currently, many contractors are weary of the FRP system mainly due to their unfamiliarity with using the product.

Rebar reinforcement retrofitting involves constructing the entire bar system on site around the column that is being retrofitted. Each longitudinal and transverse bar must be manually tied together. On a very large column, this could be very time consuming. The advantage of FRP as a retrofit method could be immense. Once the construction company is educated on the proper application of an FRP wrap or tube, it would be a time-saving process. The wrap would require the least production time, but it would allow more room for error in the application. The tubes could be mass produced if the design was more widely used, and the construction time after manufacturing would be minimal. After on-site, a wrap could be placed around the column by a construction team and attached using an epoxy resin. Another option are prefabricated tubes that could be placed around the column in sections and attached with an epoxy resin. The FRP system would eliminate the problem of tying bars and correctly aligning reinforcing bars with strict spacing and size requirements.

1.3.3 Application and Life Cycle Comparison

The life cycle of the different retrofit methods must be considered because it is the most critical aspect in the retrofitting process. A retrofit is typically done to extend the life of a structure until major repair is needed. Therefore, the product that can do this most efficiently will have an advantage over the other methods. FRP retrofitting has an advantage in this area because it has a longer life expectancy than rebar retrofitting. The FRP retrofit will be more resistant to corrosion in the construction area especially if used on a bridge pier over water. The typical rebar retrofit method has problems with durability because the cover concrete will begin to chip and crack after part of a life

cycle. If the rebar becomes exposed, it will quickly begin to corrode and lose its strength. This is a common problem in rebar retrofitting and is often the reason a retrofit application is needed for the existing structure.

All retrofit methods have their problems which is obvious considering none of them are more widely used than the other. Some problems with FRP retrofitting include its application and durability. High temperature and humidity can cause problems with the fibers and possibly cause weaknesses in the retrofit. Also, application of the FRP is difficult. The rebar retrofit jacket can be very challenging to apply on an existing column. The bending and tying of rebar is time consuming especially on a very large column. The formwork required for the concrete pour will also be very difficult to create.

The cost analysis of the two systems relies on the life cycle costs. The life cycle of a column is the most critical aspect of construction in today's society. With the number of deficient structures climbing and the resources to replace them limited, it is important to extend the life of the structures currently being built. Even with higher initial costs, the option needs to be explored.

The main problem with this analysis is that not many structures have been built using the FRP system, or rebar retrofit methods. The FRP structures that have been constructed were done so in the past ten years (Nystrom et al. 2003). An entire life cycle analysis has not been completed for the two retrofit methods, but some common ideas are agreed upon. The production costs could be lessened for FRP if it was more widely used as was

examined in Section 1.3.1. Furthermore, if the life of a structure can be extended, the larger initial costs could be recovered. Overall, it is feasible that the life cycle costs of the FRP retrofit system could be the same or better of a steel rebar retrofit.

1.4 Project Scope

Three different analytical models will be closely examined and compared with the experimental results of the FRP confined, reinforced concrete columns. The results of this analysis will be presented and experimental and analytical stress-strain diagrams will be compared. Analysis of the results will create a conclusion on the effectiveness of the experimental tests of the columns and the analytical analysis presented by the models.

1.5 Objectives

The proposed project is important for the future of retrofit and strengthening of concrete columns. There are many advantages to FRP reinforcement, but the main disadvantage is the lack of a widely accepted model that can reliably predict the behavior of the FRP confined concrete. In order to take advantage of the mechanical characteristics presented by FRP reinforcement, a design model must be proposed and used in the design of the concrete columns, along with a detailed construction technique.

This research project is aimed at aiding the process of finding a widely accepted model that can be used in the design of FRP retrofitted concrete columns. The results from the concrete column tests will be compared with the proposed models in order to show their effectiveness or ineffectiveness in predicting the strength and deformation characteristics.

Furthermore, the research project aims to show the advantages of FRP reinforcement in reinforced concrete columns as a retrofit technique. With the results of the unretrofitted column, the comparison will attempt to show the advantage of the FRP retrofit system.

1.6 Project Summary

A total of 3 analytical models developed to predict confinement provided by FRP reinforcement were compared with the results of the 3 FRP retrofitted column tests by Miller (2006) at The Ohio State University. The test columns included reinforced concrete columns retrofitted with a Carbon-FRP sheet, Carbon-FRP strips, and a Glass-FRP sheet.

This study also describes a few other models available for FRP retrofit. The analytical analysis of the 3 models examined provides some areas where application may have been a problem, some areas where the proposed model does not match the experimental data well, and some areas that represent the data set well. This project intends to further aid the understanding and development of new FRP models in the future.

CHAPTER 2

CONCRETE CONFINEMENT MODELS

2.1 Introduction

Over the last century, research has been conducted to understand the axial behavior of confined concrete, including concrete wrapped with FRP reinforcement over the past 20 years. Different researchers proposed models for concrete confined with different types of reinforcement beginning with traditional reinforced concrete. The most widely accepted model for reinforced concrete is by Mander et al (1988). This model was originally used as a starting point for FRP modeling, but it was found to over-estimate the strength of the FRP reinforcement (De Lorenzis and Tepfers 2003). A widely accepted and accurate model for FRP confined concrete is needed before the FRP products can be used as a common form of reinforcement.

2.1.1 Plain Concrete Behavior

The axial behavior of plain concrete has been widely studied by researchers for the past century, and is widely dependent on the specifications of the concrete. The water-cement ratio, cement and aggregate characteristics, concrete unit weight, type of curing and age all play a significant role in the behavior (Carreira and Chu 1985). The plain concrete

behavior is best understood from the axial compression of concrete cylinders taken from the concrete mix. Concrete gains most of its ultimate strength in the first 28 days after construction, during which time the type of curing system will affect the overall strength. The testing of the cylinders at 28 days will result in a stress-strain plot that will rise until ultimate strength and then descend quickly when the concrete crushes. Figure 2.1 shows typical stress-strain diagrams of plain concrete.

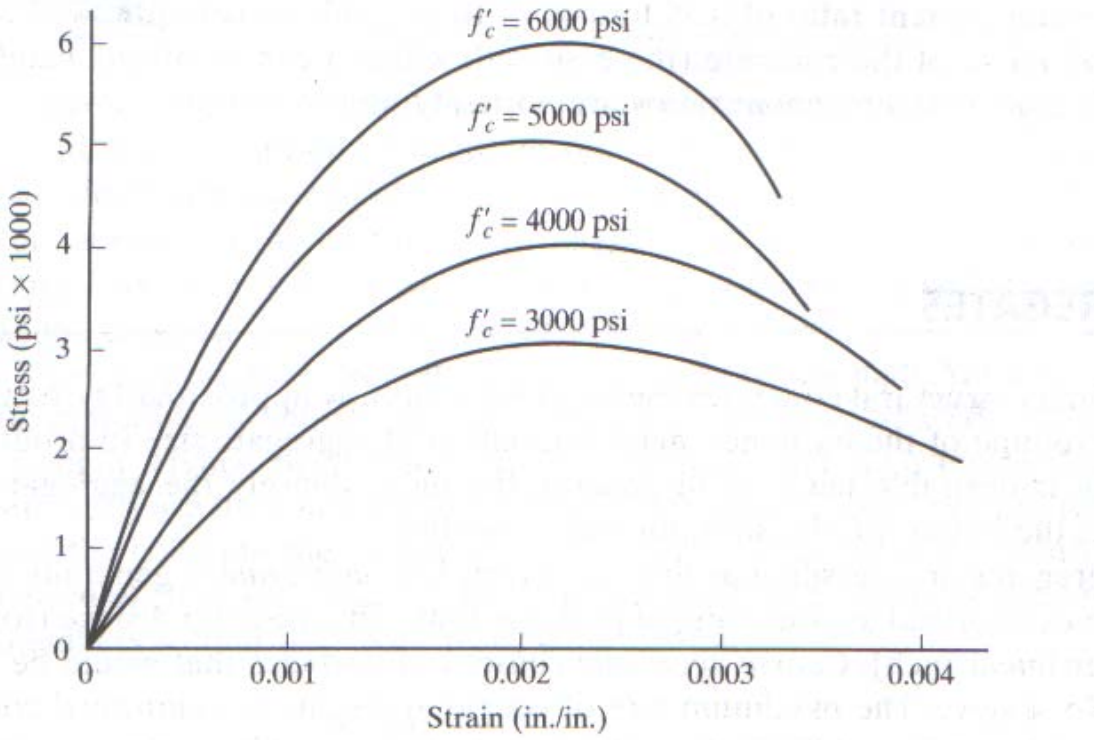

Figure 2.1 - Plain Concrete Stress-Strain Diagrams (Spiegel and Limbrunner 2003).

2.2 Concrete Confinement

Concrete confinement is a very important design factor when designing concrete columns under axial compression. Studies have shown that effective transverse confinement can cause a large improvement in axial strength and ductility of the concrete member. The

increased ductility is a desired attribute, allowing warning of structural failure in the member.

In the design of traditional rebar reinforced concrete construction, spiral reinforcement provides greater confinement than longitudinal or rectangular tie reinforcement. The best confinement can be obtained with closer spacing of the transverse reinforcement, and better distributed longitudinal reinforcement. Furthermore, the volume of transverse reinforcement should be increased in comparison with the volume of the concrete core (Mander et al. 1988). The concrete confinement is important because the cover concrete will begin to spall at a strain of 0.003 in./in. At this point, the core concrete will carry the load as long as it is effectively confined by the rebar reinforcement. The longitudinal bars will eventually begin to buckle in between the transverse reinforcement as is seen in Figure 2.2. Failure will be reached once the longitudinal and transverse reinforcement fails, and can no longer confine the concrete core (Lam and Teng 2003).

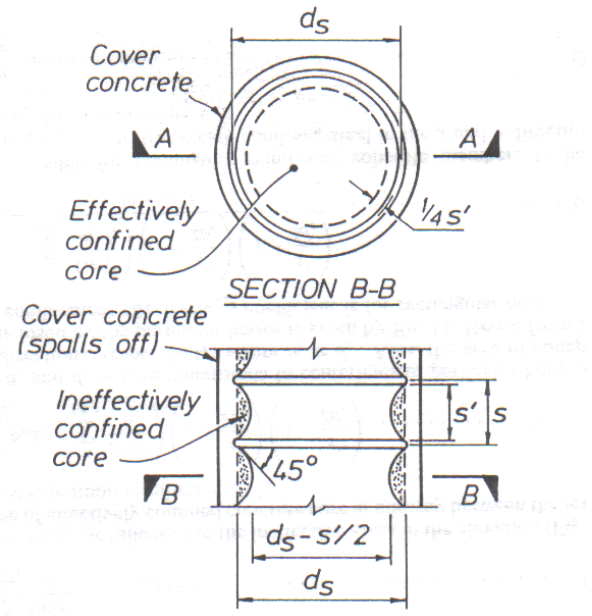

Figure 2.2 Spalling of Cover Concrete (Mander et. al. 1988).

2.2.1 Confined Concrete Behavior: Mander et al. (1988) model

For the purpose of modeling the behavior of concrete confined by steel rebar, one of the most commonly used analytical models for confined concrete columns is studied. The model was proposed by Mander et al. (1988). The model is "a unified stress-strain model for confined concrete developed for members with either circular or rectangular sections, under static or dynamic loading, either monotonically or cyclically applied" (Mander et al. 1988).

According to Mander et al. the axial concrete compressive stress, f_c, is given by Equation 2.1 where f_{cc}' is the compressive strength of the confined concrete defined in Equation 2.2, $x = \frac{\varepsilon_c}{\varepsilon_{cc}}$ and is the strain ratio. The variable r is a modulus of elasticity ratio defined in Equation 2.4.

$$f_c = \frac{f'_{cc}\, xr}{r - 1 + x^r} \qquad 2.1$$

$$f'_{cc} = f'_{co}\left(-1.254 + 2.254\sqrt{1 + \frac{7.94 f'_l}{f'_{co}}} - 2\frac{f'_l}{f'_{co}}\right) \qquad 2.2$$

The variables f'_l and f'_{co} in Equation 2.2 are defined later in this section. In the strain ratio equation, ε_c, is the longitudinal compressive concrete strain, and ε_{cc} is the strain of the confined concrete defined in Equation 2.3. In Equation 2.3, ε_{co} is the unconfined concrete

strain, and f'_{co} is the unconfined concrete compressive strength, which are assumed to be 0.002 in./in. and 4149 psi, respectively.

$$\varepsilon_{cc} = \varepsilon_{co}\left[1+5\left(\frac{f'_{cc}}{f'_{co}}-1\right)\right] \quad 2.3$$

$$r = \frac{E_c}{E_c - E_{\sec}} \quad 2.4$$

$$E_c = 57000 * \sqrt{f'_{co}} \quad 2.5$$

$$E_{\sec} = \frac{f'_{cc}}{\varepsilon_{cc}} \quad 2.6$$

In Equation 2.4, E_c is the tangent modulus of elasticity of concrete defined in Equation 2.5, and E_{sec} is the secant modulus of elasticity defined in Equation 2.6. Mander et al. defines the cover or unconfined concrete to have a stress-strain behavior following a straight line path that goes to zero at ε_{sp}, the spalling strain as shown in Figure 2.3.

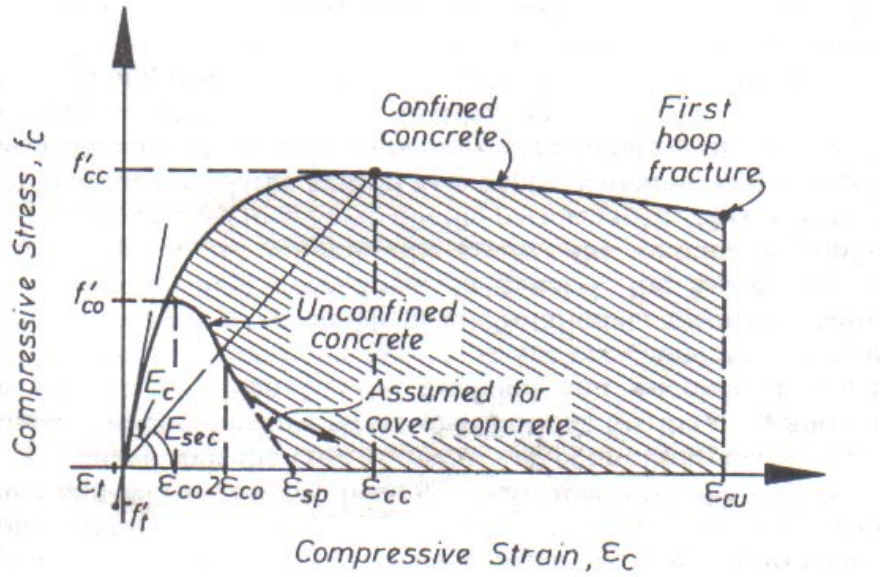

Figure 2.3 Stress-Strain Model Proposed by Mander et al. (Mander et al. 1988)

In Mander et al.'s model, an equation is used to find the confinement effectiveness coefficient, k_e, rather than using a constant as was done by Richart et al. (1928). For circular spiral reinforcement, k_e, is defined in Equation 2.7. Furthermore, Mander et al. proposed a ratio for the "volume of transverse confining steel to the volume of confined concrete core," ρ_s, which is defined in Equation 2.8. This equation includes ρ_{cc}, which is the ratio of area of longitudinal reinforcement to the area of the core section (Mander et al. 1988).

$$k_e = \frac{1 - \frac{s'}{2d_s}}{1 - \rho_{cc}} \qquad 2.7$$

$$\rho_s = \frac{4A_{sp}}{d_s s} \qquad 2.8$$

$$f_l' = \frac{1}{2} k_e \rho_s f_{yh} \qquad 2.9$$

In Equation 2.8, s, is the spacing between spirals, A_{sp} is the area of the spiral, and d_s is the diameter between the center of spirals in the transverse direction. Equation 2.9 defines the effective lateral confining stress for the concrete cylinder, f_l'. In Equation 2.9, f_{yh}, is the yield strength of the transverse reinforcement. The variables f_l' and f'_{co} can now be put into Equation 2.2 to find the compressive strength of the confined concrete, f'_{cc}.

Once f'_{cc} is calculated from Equation 2.2, it can be put into equation 2.1 to find the compressive stress. The concrete strain, ε_c, is the only factor that is varied in the model. In the model, the work done on the longitudinal steel and confined concrete in compression is used to find when the first hoop fracture occurs. According to Mander et al., "when the work done exceeds the available strain energy of the transverse steel, then hoop fracture occurs." This is the point where maximum deformation occurs. (Mander et al. 1988).

2.2.2 FRP Reinforced Concrete Behavior

FRP reinforcement is activated by the outward expansion of the crushing concrete and is therefore a passive type of reinforcement. "As the axial stress increases, the confining device develops a tensile hoop stress balanced by a uniform radial pressure which reacts against the concrete lateral expansion" (De Lorenzis and Tepfers 2003). The amount of axial load that the system can withstand relies on the FRP, when the fibers reach ultimate stress and strain the FRP system ruptures producing a brittle failure.

FRP reinforcement is essential in providing confinement to columns after the concrete starts cracking. Near failure, the concrete is cracked internally and the cracking is not uniform throughout. This also causes high stress concentrations in specific areas of the FRP reinforcement as opposed to areas where little cracking has occurred.

The FRP reinforcement is subjected to two different types of loading while the column undergoes axial deformation. There is a transverse loading from the concrete crushing and trying to push out radially. There is also some axial loading due to the epoxy resin connection between the concrete and the FRP reinforcement. This combination of loads produces strength limitations that are difficult to predict, and the failure strength of the FRP system is a portion of its ultimate strength.

Studies have shown that increasing the FRP strength and stiffness are directly related to the increase in concrete stress and strain limits. Furthermore, the strength and stiffness of the FRP is a result of the material chosen and the number of layers used. The FRP strength and stiffness are important in limiting the dilation of the concrete. Limiting the dilation of the concrete as the axial load increases will cause a rise in stress and strain capacity.

FRP confined concrete models have taken on the same general form of equations. According to Lam and Teng (2002) this general form is displayed in Equations 2.10 and 2.11 where f'_{co} = unconfined strength of concrete, f'_{cc} = confined concrete strength, ε_{cc} =

confined concrete ultimate strain, ε_{co} =unconfined concrete ultimate strain, D = dimension of concrete specimen, f_{FRP} = effective stress in FRP composite at failure of element, and t = thickness of composite jacket (ASCE 2007).

$$\frac{f'_{cc}}{f'_{co}} = 1 + k_1\left(\frac{f_1}{f'_{co}}\right)^a \qquad 2.10$$

$$\varepsilon_{cc} = \varepsilon_{co} + k_2\left(\frac{f_1}{f'_{co}}\right)^\beta \qquad 2.11$$

In equations 2.10, and 2.11 α, β, k_1, and k_2 = constants determined from individual experiments and $f_l = \frac{2f_{FRP}t}{D}$, which is equal to the confining pressure. The variable, f_{FRP}, is the effective stress in the FRP at failure. Much of the research that has been completed to this point has shown that the measured strain in the FRP is less than the maximum strain of the composite material at failure.

Many of the examined FRP models have a similar structure in how the equations are solved for. The main differences between most models are the analytical constants used. Table 2.1 gives a general overview of the models examined and provides a quick comparison of the different equation formats used. (De Lorenzis and Tepfers 2003).

Model	Theoretical fcc'	Theoretical εcc
Fardis and Khalili	$\frac{f'_{cc}}{f'_{co}} = 1 + 4.1\left(\frac{p_u}{f'_{co}}\right)^{0.86}$ $\frac{f'_{cc}}{f'_{co}} = 1 + 3.7\left(\frac{p_u}{f'_{co}}\right)^{0.86}$	$\varepsilon_{cc} = \varepsilon_{co} + 0.0005\left(\frac{E_1}{f'_{co}}\right)$
Saadatmanesh et al.	$\frac{f'_{cc}}{f'_{co}} = 2.254\sqrt{1 + 7.94\left(\frac{p_u}{f'_{co}}\right)} - 2\left(\frac{p_u}{f'_{co}}\right) - 1.254$	$\frac{\varepsilon_{cc}}{\varepsilon_{co}} = 1 + 5\left(\frac{f'_{cc}}{f'_{co}} - 1\right)$
Samaan et al.	$\frac{f'_{cc}}{f'_{co}} = 1 + 6.0 - \left(\frac{p_u^{0.7}}{f'_{co}}\right)$	$\varepsilon_{cc} = \left(f'_{cc} - \frac{f_o}{E_2}\right)$
Toutanji	$\frac{f'_{cc}}{f'_{co}} = 1 + 3.5\left(\frac{p_u}{f'_{co}}\right)^{0.85}$	$\frac{\varepsilon_{cc}}{\varepsilon_{co}} = 1 + \left(310.57\varepsilon_{fu} + 1.90\right)\left(\left(\frac{f'_{cc}}{f'_{co}}\right) - 1\right)$
Saafi et al.	$\frac{f'_{cc}}{f'_{co}} = 1 + 2.2\left(\frac{p_u}{f'_{co}}\right)^{0.84}$	$\frac{\varepsilon_{cc}}{\varepsilon_{co}} = 1 + \left(537\varepsilon_{fu} + 2.6\right)\left(\left(\frac{f'_{cc}}{f'_{co}}\right) - 1\right)$
Spoelstra and Monti	$\frac{f'_{cc}}{f'_{co}} = 0.2 + 2.2\left(\frac{p_u}{f'_{co}}\right)^{0.5}$	$\frac{\varepsilon_{cc}}{\varepsilon_{co}} = 2 + 1.25\left(\frac{E_{co}}{f'_{co}}\right)\varepsilon_{fu}\sqrt{\frac{p_u}{f'_{co}}}$
Xiao and Wu	$\frac{f'_{cc}}{f'_{co}} = 1.1 + \left[4.1 - 0.75\left(\frac{f'^{\,2}_{co}}{E_1}\right)\right]\left(\frac{p_u}{f'_{co}}\right)$	$\varepsilon_{cc} = \frac{\varepsilon_{fu} - 0.0005}{7\left(f'_{co}/E_1\right)^{0.8}}$

Table 2.1 – FRP Model Formula Comparison

2.3 FRP Confinement Models for Plain Concrete Columns

Confinement in the FRP system is easily visualized. The axial load applied on the concrete causes it to expand out radially. The FRP jacket is there to withstand this outward expansion and provide the passive confining pressure to the concrete. The FRP system will eventually fail due to the tensile stress in the lateral direction. The circular structural member provides uniform confinement with the FRP system, while a non-circular member will not be uniformly confined (Lam and Teng 2003). In the next sections, some models developed for plain and reinforced concrete confined by FRP will be presented and examined.

2.3.1 Toutanji (1999)

Toutanji was not the first to develop a concrete model for FRP confined concrete, yet his model is one of the more widely studied. Before proposing a new modeling technique, Toutanji was able to examine FRP models that had been created by other researchers. These included the first models done by Richart et al. (1928) and the widely accepted model by Mander et al. (1988) for concrete confined by conventional steel rebar.

According to Toutanji, the proposed model should only be used for short circular columns with axial loads. The behavior of the two regions of the model can be explained by two distinct features. The first region acts nearly the same way as concrete confined with steel rebar cage, due to the fact that the FRP wrap has not been activated before the concrete starts cracking. Following this at a strain of approximately 0.002, the FRP wrap is activated and the typical stress-strain curve primarily depends on the stiffness of the FRP composite. This is shown in Figure 2.4 at an axial strain of 0.2% where the experimental stress-strain curve of the three columns begins a new linear path with a much smaller slope. Also, the unconfined column fails when the FRP retrofit is activated in the other 3 columns. Toutanji found the model to produce “reliable results for the axial stress-axial strain and axial stress-lateral strain of FRP-wrapped concrete columns.” Toutanji further concluded though, “the model overestimates the axial stress of FRP-encased concrete columns.”

Toutanji’s model was based on his experimental data from 18 concrete cylinders. The experiments involved twelve FRP wrapped cylinders along with six plain concrete

cylinders. Toutanji used two layers of FRP wraps, first applying an epoxy to the dry concrete surface. Second, he applied the first layer of FRP wrap, ensuring that there was no space left between adjacent wraps. Next, a layer of epoxy was put on the first FRP wrap followed by a second FRP layer in a different direction. Finally, a layer of epoxy was added to the outside of the second layer of FRP wrap. Toutanji measured both axial and lateral strains along with the load applied at a constant rate of 0.22 MPa/sec. Results from four specimen tests are shown in Figure 2.4. The *Unconfined* column had no FRP reinforcement. Columns *C1* and *C5* were wrapped with two different Carbon-FRP sheets. Column *C1* had a larger tensile strength ultimate strain than column *C5*, but a smaller elasticity modulus and thickness. Column *GE* was wrapped in a Glass-FRP sheet that had a smaller tensile strength and elasticity modulus than either Carbon-FRP column. As can be seen in Figure 2.4, the columns followed the material properties of the FRP-reinforcement very closely. Column *C5* contained the most strain before failure, column *C1* had a very steep slope, representative of its elasticity modulus, and column *GE* was the weakest of the 3 reinforced samples.

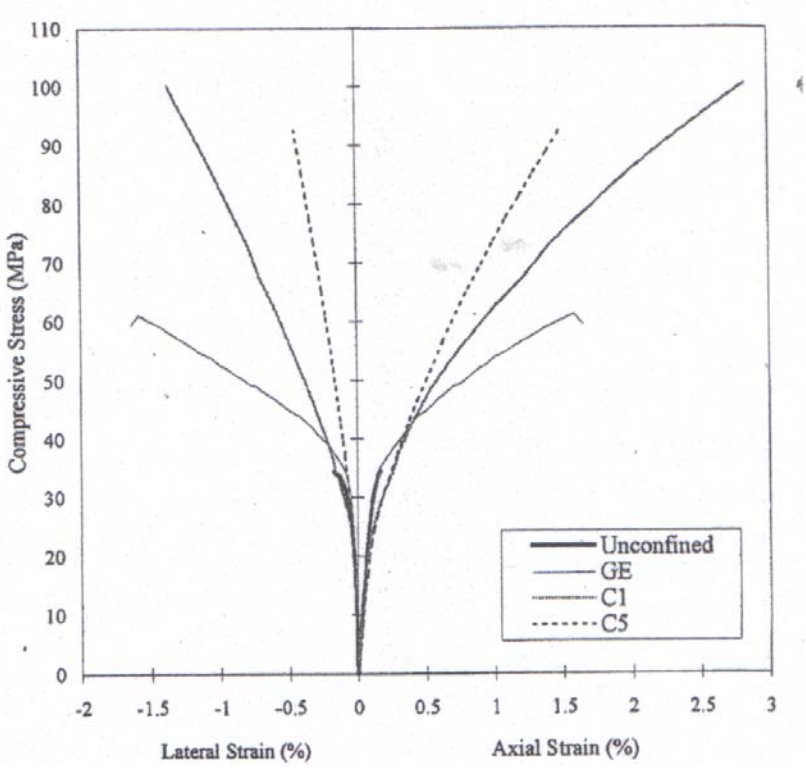

Figure 2.4 – Lateral and Axial Stress-Strain Curves found in Toutanji's Experiment (Toutanji 1999).

The analytical model proposed by Toutanji uses the basics on confinement while using the experimental results to obtain equations. Toutanji examined two regions of the stress-strain curve for FRP confined concrete separately. In the first region, the rebar reinforced concrete acts similar to the FRP confined concrete. The two methods differ greatly in the second region, which starts at a strain of 0.002 in./in.

Lateral stress in the concrete cylinder is $f_l = E_l \varepsilon_l$, where lateral elastic modulus, E_l, is calculated from Equation 2.12. The lateral strain, ε_l, is varied over the necessary range in this model. Equation 2.12 is used when the FRP is wrapped as sheets, where E_f is the elastic modulus of the fiber, t is the thickness of the FRP, and R is the radius of cylinder.

$$E_l = \left[\frac{E_f t}{R} \right] \qquad 2.12$$

Equation 2.12 becomes Equation 2.13 when the FRP is used in strips rather than sheets. In Equation 2.13, A_f is the cross-sectional area of the fiber, and S_{sp} is the distance between the center of each wrap.

$$E_l = \left[\frac{E_f A_f}{R S_{sp}} \right] \left(1 - \sqrt{\frac{S_{sp}}{2.5R}} \right) \qquad 2.13$$

To measure concrete confinement, Richart et al. (1928) proposed a variable, k_1, to calculate the axial strain in confined concrete. Through his experiments, Toutanji was able to propose an equation to replace the variable, k_1, to find the axial stress in the FRP – confined columns. Equation 2.14 displays the equation found for k_1, and Equation 2.15 is the axial stress equation, f_a, with k_1 substituted.

$$k_1 = 3.5 \left(\frac{f_1}{f_c'} \right)^{-0.15} \qquad 2.14$$

$$f_a = f_c \left[1 + 3.5 \left(\frac{f_l}{f_c'} \right) \right]^{0.85} \qquad 2.15$$

To calculate the axial strain in the concrete cylinder, Toutanji referred to models by Mander et al. (1988) and Richart et al. (1928). Similar to Equation 2.14, a new variable, k_2, was proposed by Richart et al. (1928) to perform the axial strain calculation. Once again deriving an empirical equation using his experimental results for the new variable, k_2, to replace a constant in the strain equations already proposed by Richart et al. (1928), Toutanji was able to come up with an equation for the axial strain in every point of the confined concrete. The variable, k_2, is defined in Equation 2.16 where ε_l is lateral strain. The axial strain in the region of the stress-strain curve where the FRP reinforcement has been activated, ε_a, is defined in Equation 2.17.

$$k_2 = 310.57\varepsilon_l + 1.90 \qquad 2.16$$

$$\varepsilon_a = \varepsilon_o\left[1 + (310.57\varepsilon_l + 1.90)\left(\frac{f_a}{f_c'} - 1\right)\right] \qquad 2.17$$

Toutanji modeled the first region of the proposed stress-strain curve by modifying a method proposed by Ahmad and Shah (1982) for concrete confined with steel rebar. Toutanji proposed Equation 2.18 for the stress in the concrete in the first region. The constant A_i=E_{ii}, while C_i, and D_i are defined in equations 2.20 and 2.21 respectively.

$$f_a = \frac{A_i\varepsilon_i}{1 + C_i\varepsilon + D_i{\varepsilon_i}^2} \qquad 2.18$$

$$C_i = \frac{E_{ii}}{f_{ua}} - \frac{2}{\varepsilon_{ui}} + \frac{E_{ui}E_{ii}\varepsilon_{ui}}{{f_{ua}}^2} \qquad 2.20$$

$$D_i = \frac{1}{\varepsilon_{ui}^{\ 2}} - \frac{E_{ui}\ E_{ii}}{f_{ua}^{\ 2}} \qquad 2.21$$

The variables in the preceding equations are capable of being used for both axial and lateral directions. In Equations 2.20 and 2.21 E_{ii} is the initial axial (E_{ia}) or lateral (E_{il}) elastic modulus, E_{ui} is the ultimate axial (E_{ua}) or lateral (E_{ul}) elastic modulus, ε_{ui} is the ultimate axial (ε_{ua}) or lateral strain (ε_{ul}), and f_{ua} is the ultimate axial stress. In Equation 2.20, $E_{il} = 51000(f_c')^{1/3}$, and $\varepsilon_{ul} = 0.002$. The remaining variables for Equations 2.20 and 2.21 are defined in Equations 2.22 through 2.25.

$$\varepsilon_{ua} = \varepsilon_o \left[1 + 0.0448 \left(\frac{E_l}{f_c'} \right)^{0.85} \right] \qquad 2.22$$

$$f_{ua} = f_c' \left[1 + 0.0178 \left(\frac{E_l}{f_c'} \right)^{0.85} \right] \qquad 2.23$$

$$E_{ul} = 7.557 E_l * \left(\frac{f_c'}{E_l} \right)^{0.15} \qquad 2.24$$

$$E_{ua} = 0.3075 \left(\frac{f_c'}{\varepsilon_o} \right) \qquad 2.25$$

2.3.2 Samaan et al. (1998)

Samaan, et al. recognized the overestimation involved in the typical FRP confinement model that was based off of Mander et al.'s (1988) model developed for reinforced concrete. Recognizing the fact that concrete dilation was the most important factor in developing a widely accepted and accurate confinement model for FRP, it was the most important characteristic in distinguishing their model from previous efforts.

Samaan et al. tested 30 cylindrical specimens under axial loads, and developed a new model to more closely represent the behavior of FRP confined concrete. Their comparison of several existing models is presented in Figure 2.5. As can be seen, the existing models at the time over-estimate the confinement of the FRP reinforcement.

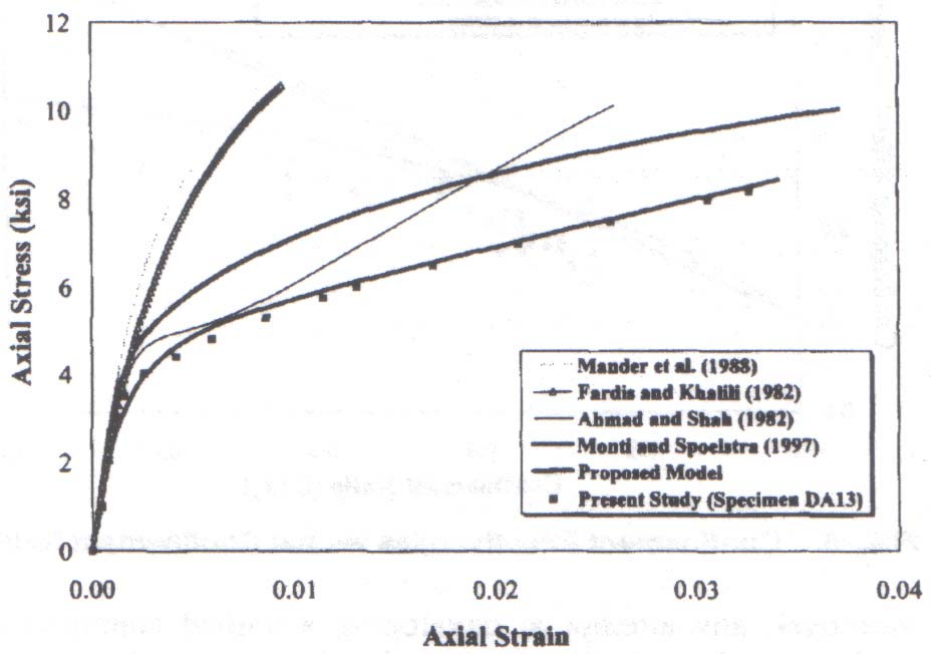

Figure 2.5 – Confinement Model Comparison (Samaan et al. 1998).

Samaan et al. proposed the use of a “four-parameter relationship” developed by Richard and Abbott (1975) that used Equation 2.26 to predict the axial strength of the concrete.

$$f_c = \frac{(E_1 - E_2)\varepsilon_c}{\left[1 + \left(\frac{(E_1 - E_2)\varepsilon_c}{f_o}\right)^n\right]^{1/n}} + E_2\varepsilon_c \qquad 2.26$$

In this equation, f_c = axial stress of the concrete, ε_c = axial strain of the concrete, E_1 and E_2= first and second slopes of the curve respectively, f_o = stress at the intercept of the second curve with the stress axis, and n = a parameter that specifies the curvature through the transition zone. To include the effect of confinement, Samaan et al. used Equation 2.27 where f'_{cu} is the confined strength of concrete, f'_c is the unconfined strength of concrete, k_1 is the coefficient of effective stiffness to be defined later, and f_r is the confinement pressure defined in Equation 2.28

$$f'_{cu} = f'_c + k_1 f_r \qquad 2.27$$

$$f_r = \left(\frac{2 f_1 t_j}{D}\right) \qquad 2.28$$

In equation 2.28, t_j is the thickness of the tube or wrap, f_j is the hoop strength of the tube, and D is the core diameter of the cylinder.

To find the coefficient of effective stiffness, Samaan et al. studied older models that used constant values for k_1 that led to inaccurate predictions. Using the test results of Samaan et al.'s current study, they derived k_1 in Equation 2.29 and used it in Equation 2.27 for the FRP confined strength of concrete.

$$k_1 = 3.38 f_r^{0.7} \qquad 2.29$$

Samaan et al. used the same equation as Ahmad and Shah (1982) to model the first linear curve and stiffness, E_1 presented in Equation 2.30. The second curve is modeled from the equation for stiffness, E_2 shown in Equation 2.31. This was found empirically using the results of the experiments completed by Samaan et al, where E_j = effective modulus of elasticity of the tube in the direction of the hoop.

$$E_1 = 47.586\sqrt{1.000 f'_c} \qquad 2.30$$

$$E_2 = 52.411 f'^{0.2}_c + 1.3456 \frac{E_j t_j}{D} \qquad 2.31$$

The stress at the intercept of the two linear curves for FRP reinforcement shown previously Figure 1.2 is given by Equation 2.32 for the Samaan et al. model. The ultimate strain, ε_{cu}, is given in Equation 2.33.

$$f_o = 0.872 f'_c + 0.371 f_r + 0.908 \qquad 2.32$$

$$\varepsilon_{co} = \frac{f'_{cu} - f_o}{E_2} \qquad 2.33$$

The proposed confinement model by Samaan et al. effectively predicts the stiffness of the FRP wrap in proportionality to the second curve of the model. The model displays the yielding at the limit of the unconfined concrete strength. This is where the load is being transferred to the FRP reinforcement (Samaan et al. 1998).

2.3.3 Other Models for FRP Confined Concrete

Spoelstra and Monti (1999) developed a confinement model not only for FRP reinforcement but also for steel jackets or other transverse reinforcement. The model presented by Spoelstra and Monti is not an empirically based model like many others presented here. It uses an iterative approach. The model keys on the interaction between the dilating concrete and the confining device, in this case the FRP. Spoelstra and Monti claim that their model is able to trace the strain in the jacket and detect its failure. Their model predicts the response of the test columns closely (Spoelstra and Monti 1999).

As some of the earliest researchers to investigate FRP confined concrete, Fardis and Khalili (1982) proposed a curve that would be able to closely approximate the response of the FRP confined concrete. Fardis and Khalili did not recommend an analytical model in their early research in 1982. However, they did propose that the response of the FRP confined concrete be modeled as a bilinear response. Fardis and Khalili proposed that the linearity of the initial curve should stop at a strain of 0.003, which is an estimate of the

peak stress of unconfined concrete. At this point the second half of the bilinear curve would begin, representing the portion of the response in which the FRP reinforcement was fully activated (Fardis and Khalili 1982). While the proposed curve is similar to the more recent models, it was found to severely underestimate the ultimate strains in the concrete (De Lorenzis and Tepfers 2003).

Saadatmanesh et al. (1994) developed an FRP confinement model that was created based off of the Mander et al. (1988) model for reinforced concrete discussed earlier in Section 2.2.1. To model the ultimate strain of the concrete column, an "energy balance approach" was employed in which the ductility available and the energy stored in the confined concrete are compared (De Lorenzis and Tepfers 2003). The comparison produces a prediction on the ultimate stress and strain of the concrete column. Saadatmanesh et al. noted that the rate at which the ultimate parameters of the concrete are reached can be slowed with a higher concrete compressive strength. Also, ductility can be increased with an increase in the thickness of the FRP wrap (Saadatmanesh et al. 1994).

The research done by Pantazopoulou and Mills (1995) relates closely to the work completed by Spoelstra and Monti (1999). The most important aspect of this model is the link that is created between lateral and axial strains in the system, and the confinement of the concrete. The proposed model uses Mander et al.'s equations to develop stress-strain curves for varying confining pressures. The one characteristic that singles out this model is its ability to predict the descending branch of the stress-strain curve, after ultimate stress and strain have been reached. Pantazopoulou and Mills also developed approximate

equations that can be used to obtain ultimate stress and strain in the model (De Lorenzis and Tepfers 2003).

Saafi et al. (1999) also worked on a model that was nearly the same as Toutanji (1999). However, the model by Saafi et al. was based on experimental data from cylinders within FRP tubes, rather than FRP wraps. Saafi et al.'s model was not used in this analysis because it was developed for FRP tubes, not wraps. The main difference that this created was in the constants used. The better bond is gained from the FRP wraps with the concrete column as opposed to the FRP tube and the column (De Lorenzis and Tepfers 2003).

Another bilinear axial stress-strain relationship for FRP reinforcement was proposed by Xiao and Wu (2000). The equations presented in this model were developed using the column test data. This model is criticized in that it fails to recognize early failure of the FRP. Many of the test specimens failed in the range of 50-80% of the ultimate strain observed in the coupon tests of the FRP material.

2.4 FRP Confinement Models for Reinforced Concrete Columns

2.4.1 Matthys et al. (2006)

The model proposed by Matthys et al. is one of the few models available that used the FRP wrap to confine reinforced concrete columns. Others include Hosotani et al. (1997), Harries et al. (1998), Demers and Neale (1999), and Wang and Restrepo (2001). These

models did not closely match the experimental design and test methods used by Miller (2006) and were not examined further in this analysis.

All of the previous models discussed in Section 2.3 used FRP as a reinforcing mechanism for plain concrete columns. Matthys et al.'s study was one of the first studies to test large-scale reinforced concrete columns. The columns were 2 m (6.56 ft) tall and 400 mm (15.75 in.) in diameter. Matthys et al. was able to conclude from their research that a larger axial stiffness in the FRP wrapping correlated to a smaller ultimate axial strain and smaller ductility. Matthys et al. also found from their large-scale columns that previous small scale models by Spoelstra and Monti (1999), and Toutanji (1999) were very close to their results.

In developing a stress-strain model, Matthys et al. proposed a modified form of the Toutanji model presented in Section 2.3.1. One of the proposed changes was the lateral stress equation. Matthys et al. noted that the hoop rupture strain was approximately 60% of the FRP ultimate strain, therefore producing his proposed Equations 2.34 and 2.35.

$$f_l = \frac{2t_f E_f \varepsilon_{clu}}{D} \qquad 2.34$$

$$\varepsilon_{clu} = \beta \varepsilon_{fu} \qquad 2.35$$

Where, ε_{clu} is the adjusted strain, β is the reduction factor equal to 0.6, and ε_{fu} is the ultimate strain in Equation 2.35. This produces the revised Toutanji model, Equation 2.36.

$$f_a = f_{co}' \left[1 + 2.3 \left(\frac{f_l}{f_{co}'} \right)^{0.85} \right] \qquad 2.36$$

All other previously described equations of the Toutanji model in section 2.3.1 remain the same as those described in Section 2.3.1, including those for the first linear curve of the stress-strain model (Matthys et al. 2006).

CHAPTER 3

EXPERIMENTAL TEST DATA

3.1 Introduction

The experimental data used in this study was collected by Miller (2006), a former Graduate Student at The Ohio State University. Miller (2006) tested circular columns in compression and obtained load-displacement data for the 3 Fiber-Reinforced Polymer columns along with 14 other columns including a "Base" or unretrofitted column.

3.1.1 Summary of Experimental Research by Miller (2006)

A total of three reinforced concrete columns with an FRP retrofit were tested as part of a previous research project. This project involved 17 reinforced columns and was conducted by Miller (2006) at The Ohio State University. There was one control column or "Base" column that was not retrofitted by FRP and is shown in Figure 3.1. All of the specimens had a height of 30 in. and a diameter of 6 in. The longitudinal reinforcement was provided by six - #3 rebar at 30 in. lengths. All of the columns were reinforced by ¼ in. diameter spiral rebar in the transverse direction. The vertical spacing between the spirals was 3 in. The outside diameter of the reinforcement was 5 in., ensuring ½ in. clear

concrete cover over the steel reinforcement. The longitudinal and transverse reinforcement were tied together with tie wire (Miller 2006).

Figure 3.1 – Base Columns Before Retrofitting (Miller 2006).

The first reinforced concrete column was retrofitted with a Carbon fiber fabric referred to as SikaWrap® Hex 103C provided by the Sika® Corporation. This composite product was applied to the reinforced concrete column as one sheet using an impregnating resin Sikadur® 300, also provided by the Sika® Corporation. This concrete column was named C-CFRP (Miller 2006) and is shown in Figure 3.2(a).

The second column was wrapped in strips of the same carbon FRP, rather than one sheet as in the first column. A picture of this column, named C-CFRP-ST is shown in Figure 3.2(b).

The third column was wrapped using a glass fiber fabric. This glass fiber fabric is named SikaWrap® Hex 107G. The fabric was also applied to the concrete column using Sikadur® 300. An undamaged picture of this column, C-GFRP, is shown in Figure 3.2(c).

a.) C-CFRP (b) C-CFRP-ST (c) C-GFRP

Figure 3.2 – Reinforced Concrete Columns Retrofitted with FRP (Miller 2006).

3.2 Test Data

The load-displacement plots for the three FRP retrofitted specimens and the base column are presented in Figure 3.3. The axial stress was calculated by dividing the applied axial load by the gross cross-sectional area, A_g = 28.28 $in.^2$ (Stress = $\frac{P}{A_g}$). The strain is equal

to the measured displacement divided by the total length, 30 in. The subsequent stress-strain plots for the four columns are presented in Figure 3.4.

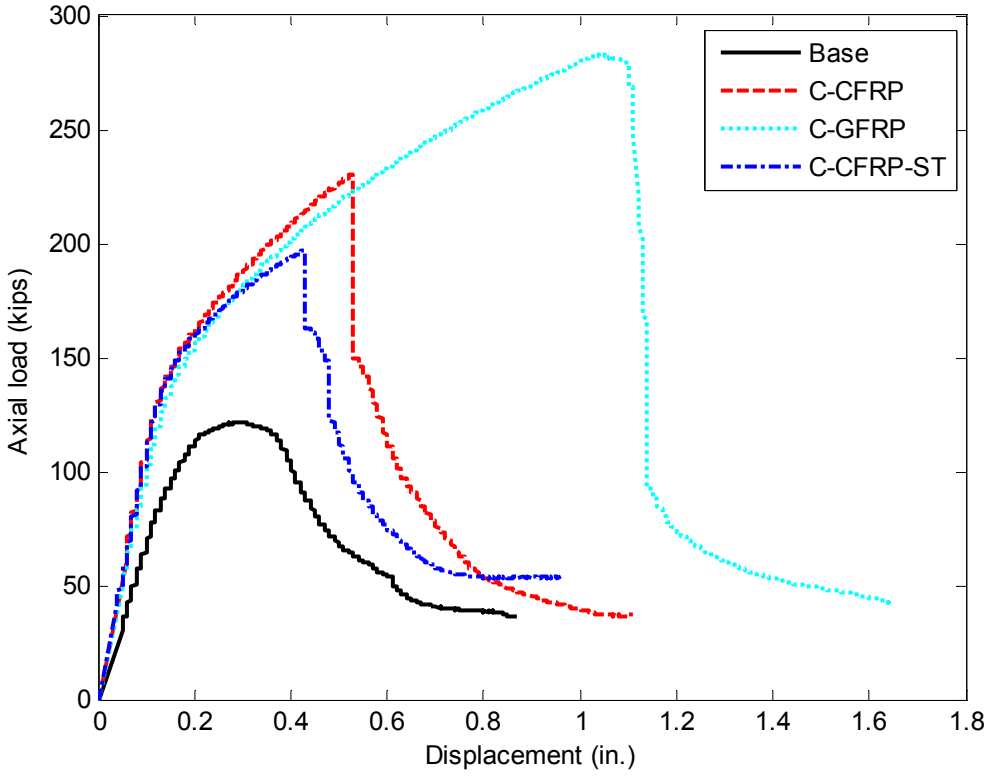

Figure 3.3 – Load-Displacement Plots for Test Columns Base, C-CFRP, C-CFRP-ST, and C-GFRP.

Figure 3.3 clearly shows the increase in strength and deformation capacity of the columns due to the FRP retrofit. The glass-FRP provided the largest strength and deformation increase among the 3 retrofit columns. The C-GFRP column was able to undergo a displacement of nearly 1.1 inches or approximately 3% of its entire length before failing by fracture of the FRP. The maximum displacement at failure was approximately 0.55 in.

for C-CFRP and 0.45 in. for C-CFRP-ST. The “Base” column only withstood approximately 0.3 in. of deflection when its ultimate strength was reached.

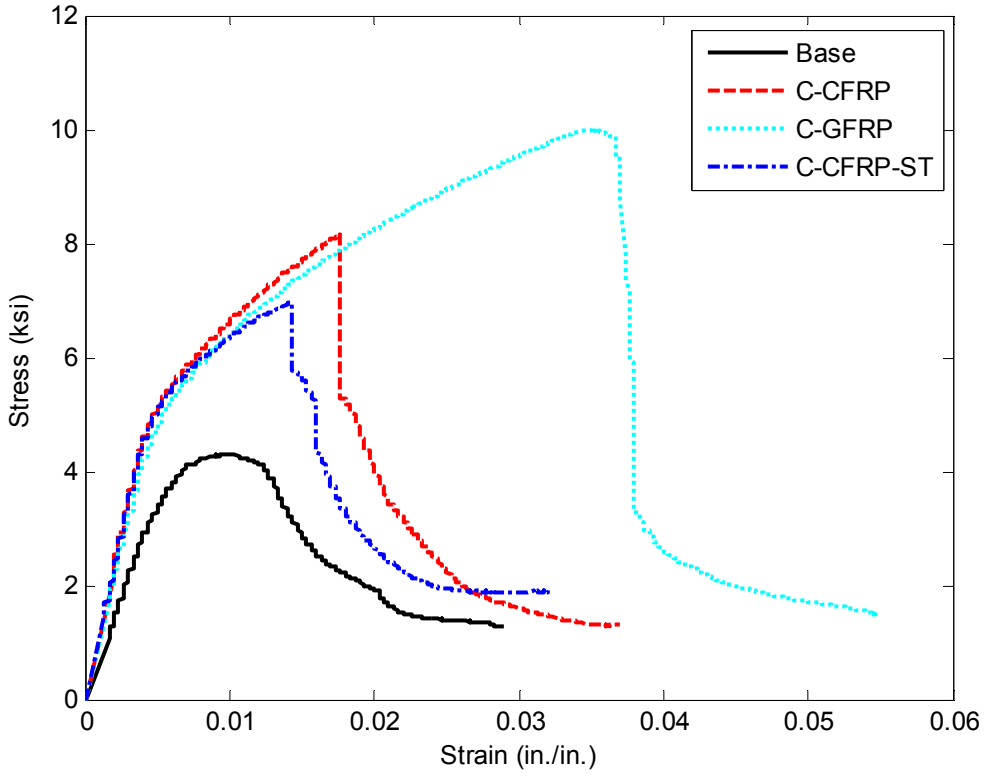

Figure 3.4 – Stress-Strain Plots for Test Columns Base, C-CFRP, C-CFRP-ST, and C-GFRP.

Figure 3.4 shows the impact of the FRP reinforcement on the column behavior. It is shown that the FRP retrofitted columns have larger strength than the “Base” column. The two different behavior regions are easily distinguishable. The first region represents elastic behavior up to a strain of about 0.004 in./in. where the transition to the second region starts. In this region, the concrete dilation is negligible and the FRP is stressed significantly.

The second zone, starting at a strain of approximately 0.004 in./in. in Figure 3.4, is where the behavior of FRP reinforced columns differ greatly from the unretrofitted “Base” column. In this region, the concrete dilation begins as the reinforced concrete column begins to crack and fail under increasing axial load. The FRP retrofit provides lateral support to allow the column to resist a larger load without failing. However, in the Base column, failure occurs once the peak strength is reached and followed by gradual strength depreciation. The FRP retrofitted columns have a second response on the graph between a strain of 0.004 in./in. and brittle FRP fracture that may be approximated by a linear line.

As shown in Figure 3.5, all three failures of the C-CFRP, C-GFRP, and the C-CFRP-ST columns were brittle. The failure of the FRP composite happens when only one section of the wrap fails. When the FRP specimens failed, a large popping sound was created. It was a result of the fracture of fibers in the composite wrap. This type of brittle failure is undesirable in the design of structures. It is critically important to know the fracture strength of FRP reinforcement, so the failure point could never be approached during the life of the FRP reinforced structure.

Two conclusions are apparent from Figure 3.5. The first conclusion is that all three specimens experienced brittle failure. The second is that the FRP in all three specimens fractured at one location, while the rest of the specimen shows very little sign of damage. With FRP reinforcement, there is no cover concrete spalling, gradual strength degradation, or steel yielding as in the “Base” column to provide warning that the column

is near failure. The FRP reinforcement conceals the warning signs, and this is a concern when using FRP reinforcement. A second concern is that if one small area of the FRP reinforcement is not applied properly, the strength of the entire column will be compromised.

a.) C-CFRP b.) C-CFRP c.) C-CFRP-ST

Figure 3.5 – Columns After Loading and Failure (Miller 2006).

CHAPTER 4

ANALYTICAL RESEARCH

4.1 Introduction

The following section gives an overview of the effectiveness of proposed theoretical models and how they compare with the experimental results found in the experiment. It is the intent of this project to determine the effectiveness of the analyzed models in predicting the strength of concrete columns confined with an FRP composite. The following models are only a sample of the numerous proposals done by researchers on the topic of FRP reinforcement. However, they were chosen carefully because of their close relationship with the specifications proposed in this project.

4.2 Results of Theoretical Models

4.2.1 Mander et al. (1988) Model Results and Comparison

The widely recognized model by Mander et al. was used to model the Base column in the experiment that was not retrofitted with FRP reinforcement. It was decided to model the "Base" column to compare how the "Base" column would match up to a widely accepted confined concrete model. Also, the performance of the "Base" column should be similar to the confined concrete columns in the FRP retrofitted columns.

The experiment performed by Miller (2006) included a slow strain rate and a monotonic loading. There was no dynamic loading and the test specimens were circular. The model by Mander et al. can be used for confined and unconfined concrete specimens. The concrete strength of the base column was 4149 psi at the time of testing. This number was reached by the breaking of two concrete cylinders the day of testing and averaging the results together (Miller 2006). Due to the retrofit technique, the cover concrete must be considered unconfined concrete, and its gross area must be treated differently than the confined concrete. Using the equations described in Section 2.2.1, Figure 4.1 was developed to find the axial stress in the confined and unconfined concrete.

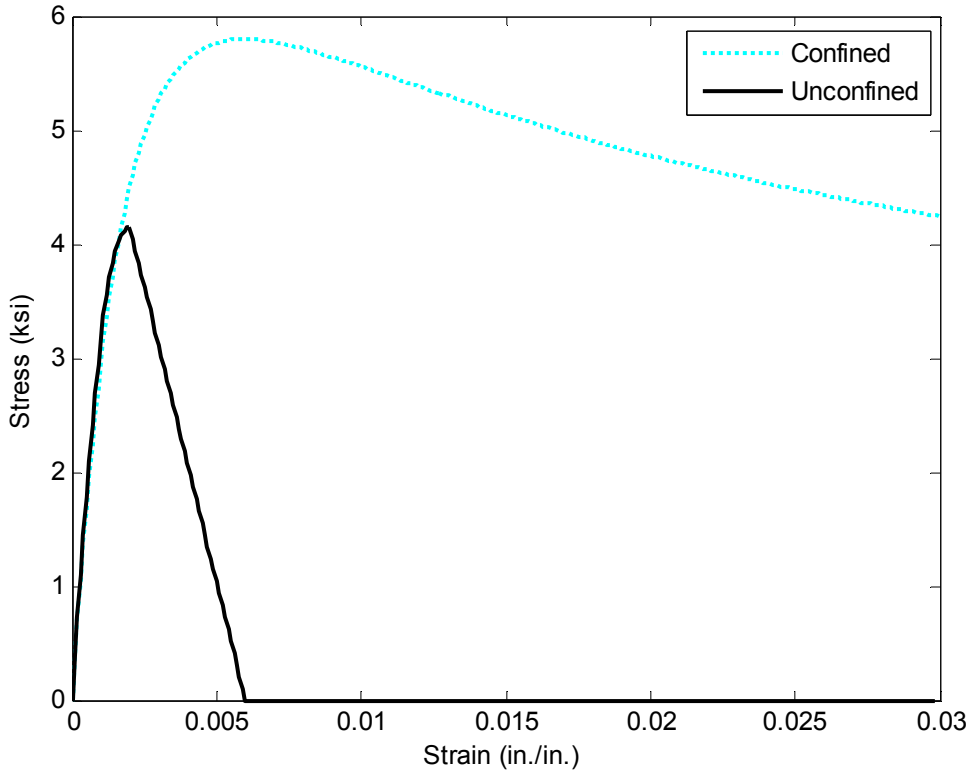

Figure 4.1 - Theoretical Stress-Strain Plot of Confined Concrete vs. Unconfined Concrete for Mander et al.'s model

The ultimate stress difference between the unconfined and confined concrete is about 2 ksi, and the difference in strain was about 0.005 in/in. The unconfined concrete model uses a straight-line curve from the ultimate strain of 0.002 to the spalling strain 0.006. These two strain values are common assumptions.

The Load displacement for Mander et al.'s model is developed using the equation $P = f_{unconfined} * A_{cover} + f_{confined} * A_{core}$. Where, $f_{unconfined}$ is the axial stress of the unconfined concrete, A_{cover} is the cross sectional area of the unconfined concrete, $f_{confined}$ is the axial stress of the confined concrete, and A_{core} is the cross-sectional area of the confined concrete. Using the specifications provided by Miller for the construction of the rebar cages, and the equation for the loading, *P*, the resulting Load-Displacement curve in Figure 4.2 is produced.

Figure 4.2 was created to show the difference in Mander et al.'s predicted model and the "Base" column. This is important because the base column should have very similar behavior to the base columns in the FRP retrofitted columns. Mander et. al's model does a good job of predicting the behavior of the unretrofitted "Base" column. The obvious difference is that the "Base" column experienced a much larger displacement before reaching its ultimate load than was predicted.

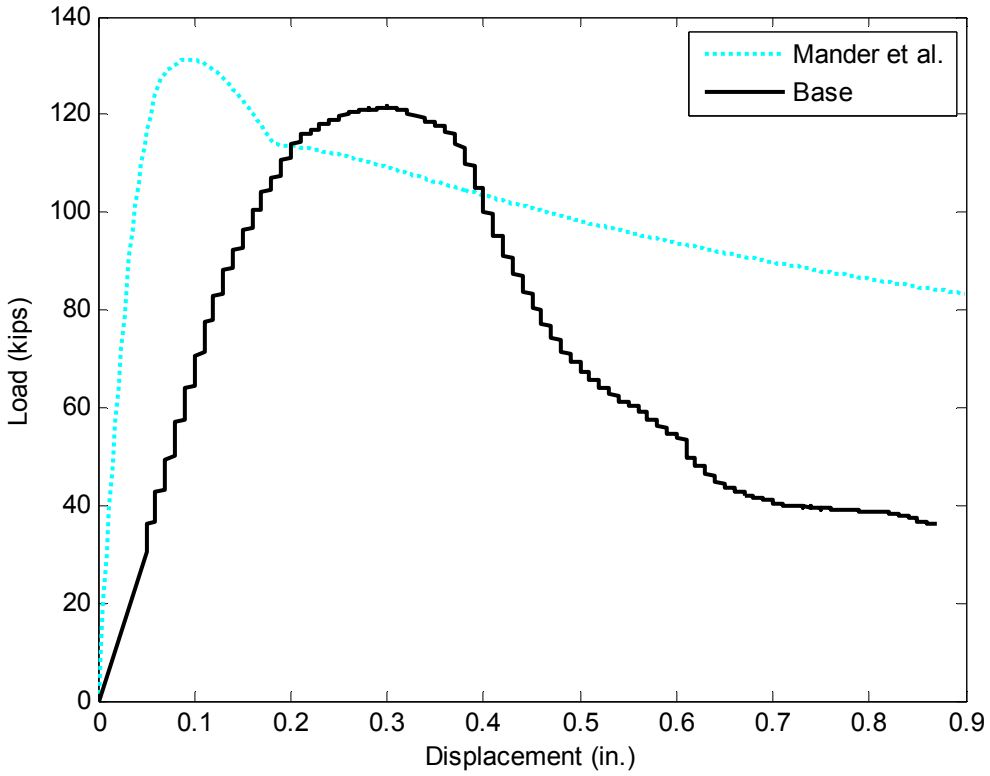

Figure 4.2 – Load –Displacement Plot of Base Column vs. Mander et al.'s model

4.2.2 Toutanji (1999) Model Results and Comparison

The model developed by Toutanji (1999) was compared to the test results found from the experimental columns wrapped with fiber-reinforced polymer composite. Toutanji's model differs from other models in its lack of the use of analytical constants. Instead, Toutanji used lateral strains he found in his experiment to develop equations for these constants. Therefore, the lateral strains had to be assumed in this project over a range that made the model comparable to the experimental data. The elastic modulus of the glass and carbon FRP was found from the product data sheet provided by the supplier, Sika®. The elastic modulus for glass, E_{fg} = 10,500,000 psi, and the elastic modulus for carbon,

E_{fc} = 34,000,000 psi. For the first region of the stress-strain curve, to a maximum strain of 0.002, the Toutanji model was not used. It was decided that this was not the point of interest in the experiment. Equation 4.1 was used to model the elastic section of the stress-strain graph.

$$f_a = E\varepsilon_a \qquad 4.1$$

The stress-strain graph of the carbon-FRP modeled against the experimental carbon sheets column (C-CFRP) and the base column (Base) is provided in Figure 4.2.

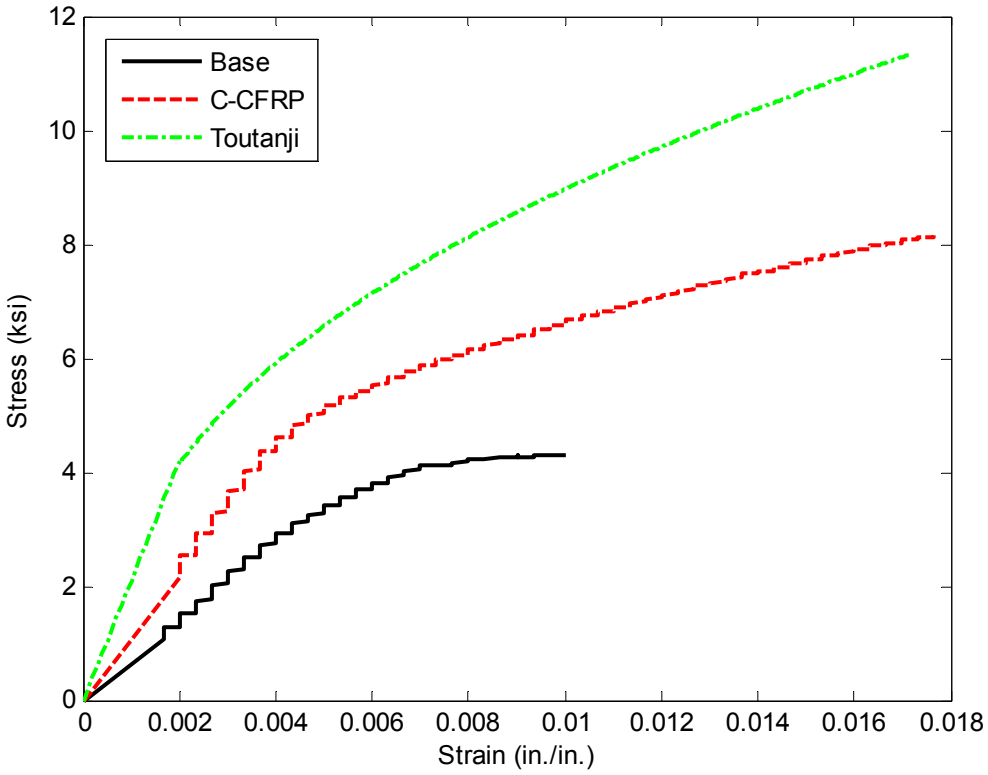

Figure 4.3 Theoretical Stress-Strain Plot of Carbon-FRP sheets for Toutanji's Model vs. Experimental Columns C-CFRP and Base

The stress-strain graph of the carbon-FRP strips modeled against the experimental carbon composite strips column (C-CFRP-ST) and the base column (BASE) is provided in Figure 4.3.

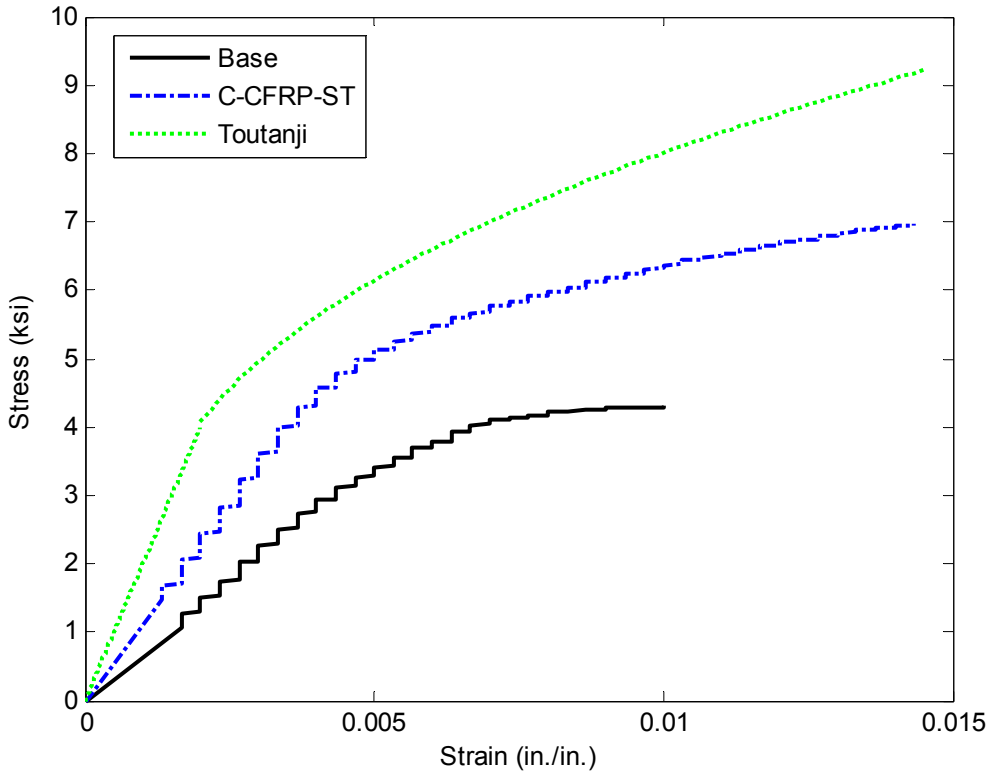

Figure 4.4 Theoretical Stress-Strain Plot of Carbon-FRP Strips for Toutanji's Model vs. Experimental Columns C-CFRP-ST and Base

The stress-strain graph of the Glass-FRP (Toutanji) modeled against the experimental glass composite sheets column (C-GFRP) and the base (Base) column is provided in Figure 4.4.

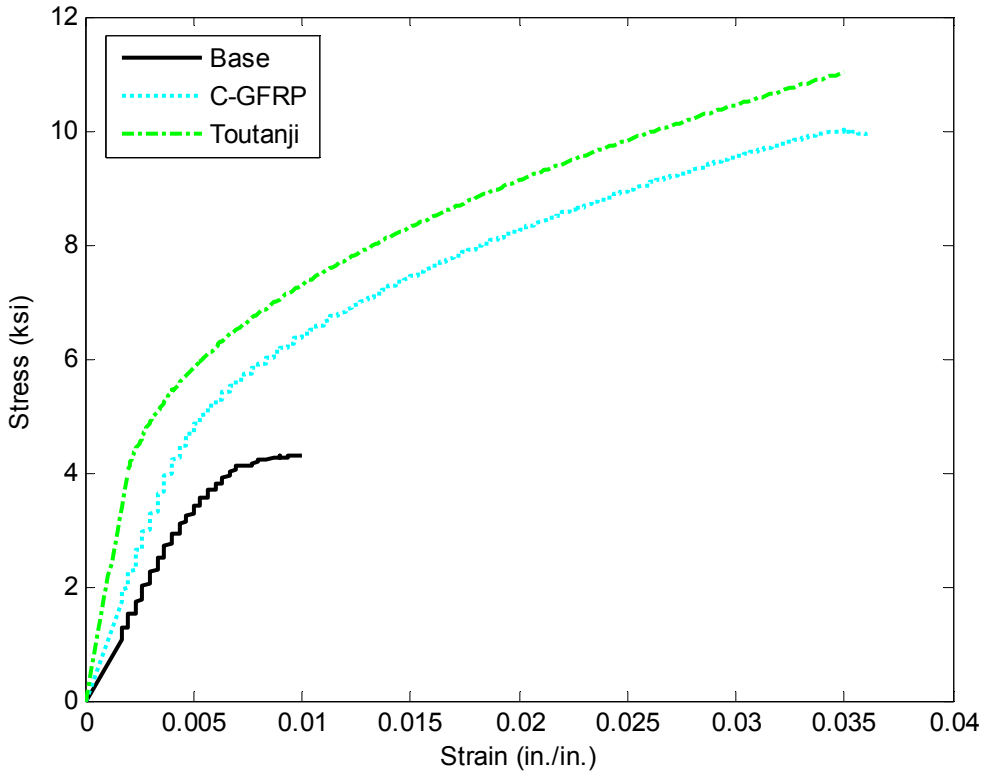

Figure 4.5 Theoretical Stress-Strain Plot of Glass-FRP sheets for Toutanji's Model vs. Experimental Columns C-GFRP and Base

All of the Carbon-FRP theoretical models proposed by Toutanji over-estimate the impact of the FRP composite on the confinement of the reinforced concrete column. This is most evident in Figures 4.3 and 4.4 for the Carbon-FRP sheets and strips. The theoretical model over-estimates the strength of the column at failure by about 3 ksi. It must be noted that some of the discontinuity can be attributed to human error. It is likely that there may have been some inconsistencies in the application due to inexperience in using the material (Miller 2006). However, it is likely incorrect to assume that all the error can be attributed to the lack of application experience.

In the analysis of the only columns that used carbon strips, rather than sheets for reinforcement, one can also note the over-estimation of the theoretical model. Although only about 2.5 ksi at failure, the difference is too large to be an accepted solution for this column. However, it should be noted that since the FRP strips were more difficult to apply, the human error involved in application would be larger in this case.

The Glass-FRP column in Figure 4.5 represents the best evidence of Toutanji's model being acceptable. The smaller elastic modulus in the glass-FRP composite brings the theoretical model much closer to the actual results with a difference in stress of 1 ksi at failure. While this is still unacceptable in application, it provides insight into the fact that Toutanji's model may be more accurate than the results show. Figure 4.5 almost exactly models the second linear curve during the portion of the experiment when the FRP is activated. The theoretical and experimental lines are only slightly different from one another because the theoretical model assumed the concrete "Base" column to resist more load before requiring the FRP reinforcement to activate. This problem was expected after the model by Mander et al. was completed and analyzed in Section 4.2.1.

Human error may have been more of a problem than originally thought in the application of the carbon-FRP reinforcement. According to the specifications for the wraps provided by the Sika Corporation, the supplier of the FRP composite, the modulus of the carbon-FRP is much higher than the glass-FRP. It is apparent that an error may have occurred involving the carbon-FRP. Due to its higher modulus, it should have been stronger in the testing than the glass-FRP, which it was not.

Toutanji's model appears to be relatively close in modeling the FRP composites. Toutanji stated in closing his paper, "the model overestimates the axial stress of FRP-encased concrete columns" (Toutanji 1999). This over-estimation is true in this case and does not allow the model to be recognized as acceptable, but still provides good basis for further research.

4.2.3 Samaan et al. (1998) Model Results and Comparison

The model presented by Samaan et al. was tested against the results of the three reinforced concrete columns, C-CFRP, C-CFRP-ST, and C-GFRP. The model required the use of the material properties of both the carbon and glass FRP materials. Through the data sheet provided by the Sika® Corporation, the following values were found. The hoop strength of the tube, f_j, for the carbon and glass FRP was 123.2 ksi and 94 ksi respectively. Furthermore, the effective modulus of elasticity of the FRP reinforcement, E_j, for the carbon and glass FRP was 10,239.8 ksi and 3,794.1 ksi respectively. The concrete compressive strength, f'_c, was found to be 4149 psi, as was tested and reported by Miller (2006).

In the Samaan et al. model, there is no change in models for FRP sheets or strips. Therefore, there was no difference between models for the carbon strips or sheets and the results of the model are shown in Figure 4.6.

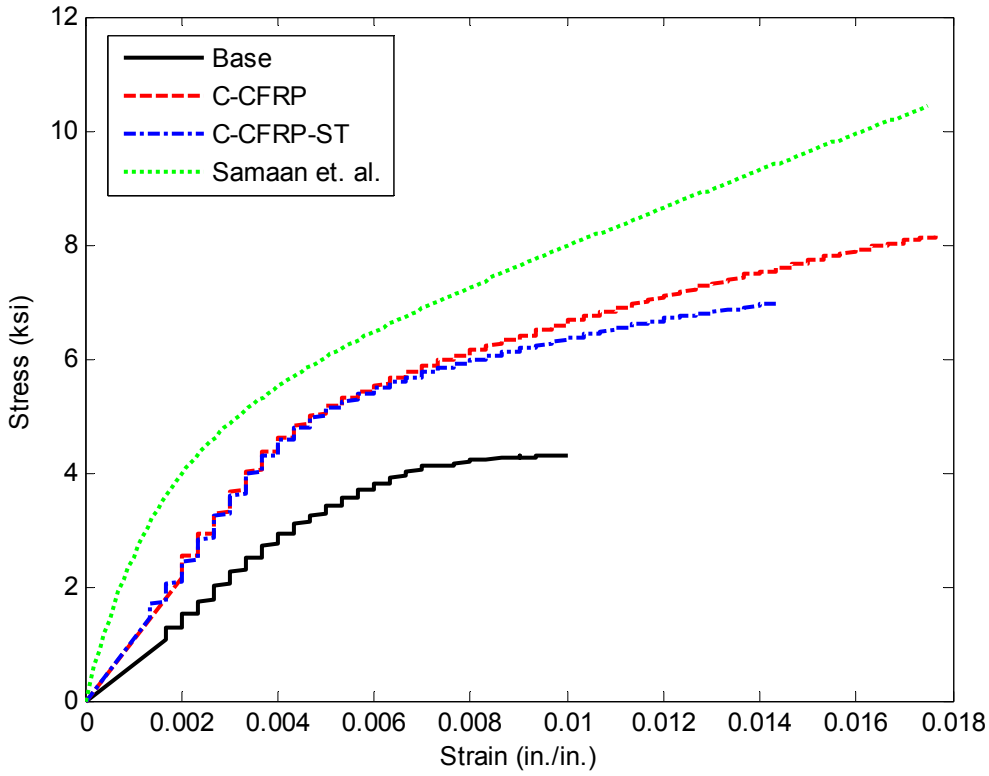

Figure 4.6 – Theoretical Stress-Strain Plot of Carbon-FRP for Samaan et. al.'s Model vs. Experimental Columns C-CFRP, C-CFRP-ST, and Base

The model by Samaan et al. overestimates the experimental results found from the experiment. As stated in the previous section, these results could be low from human error in the application of the FRP materials, especially on the sample with the CFRP strips where more room for inconsistencies is present.

In a similar result, the model for the glass-FRP column over-estimates the actual strength seen in the experiment. The resulting stress-strain curves can be seen in Figure 4.7.

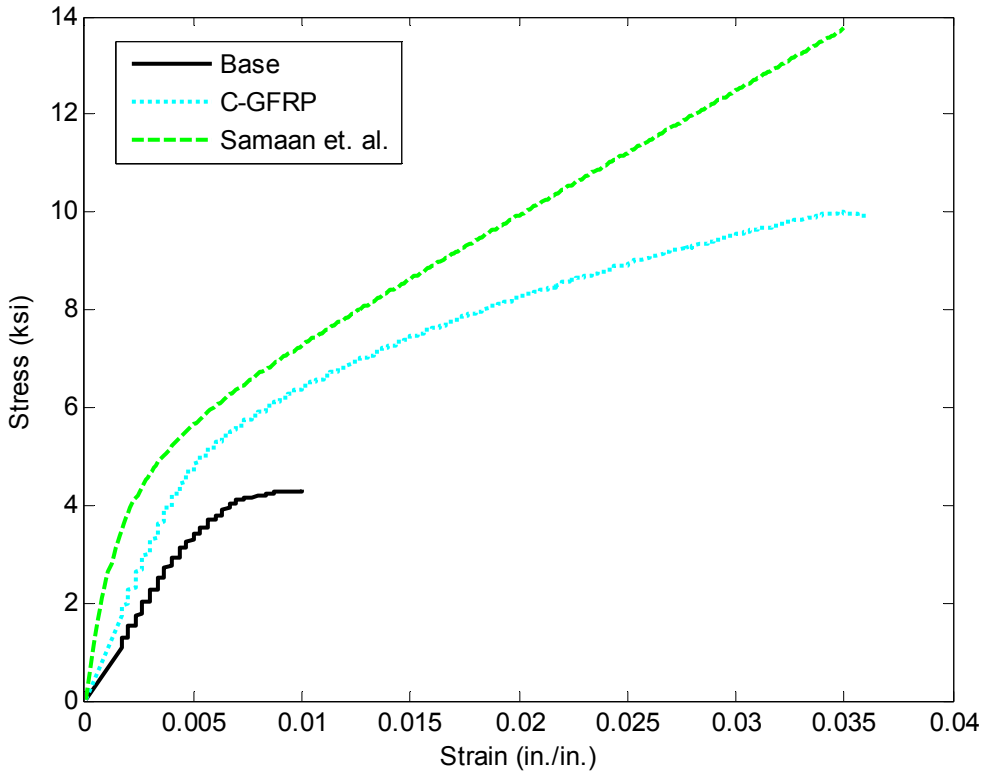

Figure 4.7 – Theoretical Stress-Strain Plot of Glass-FRP for Samaan et. al.'s Model vs. Experimental Columns G-CFRP and Base

The resulting plots presented here display the gross error that could be present if the model were used in the design of FRP reinforced columns. At the failure strain of approximately 0.035 in./in., the model over-estimates the stress in the glass-FRP by about 4 ksi. Inconsistencies exist in both the first and second linear portions of the graph. The experimental column has smaller slope in both sections than the theoretical stress-strain curve. This causes the predicted and experimental values to have more deviation as the strain increases. However, in contrast to the Toutanji model, most of the deviation between the theoretical and proposed curves in the Samaan et al. model exists in the second linear portion of the curve. As stated previously, this is the portion of the curve at

which the FRP reinforcement is activated and critical. Therefore, the Toutanji model does a better job of actually predicting the FRP reinforcement than the Samaan et al. model in Figure 4.7

4.2.4 Matthys et al. (2006) Model Results and Comparison

The model by Matthys et al. was a modified version of the Toutanji model that was described earlier. This model was actually a result of a study done on FRP for reinforced concrete columns, rather than plain concrete like the previous analytical models discussed. For this reason, this model was used in this analysis.

The model proposed by Matthys et al. performed better than the previous models by Toutanji and Samaan et al. Three plots were created because the model changes for the FRP strips and sheets. The result of the carbon-FRP model is presented in Figure 4.8.

Figure 4.8 displays the relatively small over-estimation of the Matthys et al. model in predicting the stress-strain characteristics of the carbon-FRP column. The difference between the experimental and theoretical results is less, however, than the Toutanji or Samaan et al. models. At the maximum strain of 0.018 in/in, there is only a 1 ksi difference between the theoretical and experimental results. While this error prevents this model from practical use, it is much closer than the previous models discussed. Another encouraging fact in this model is that most of the differences between the experimental and theoretical curves exist in the first linear portion of the graph, before the FRP reinforcement has been activated. This is encouraging because this is the part of the curve

that is more easily predictable. It is the second linear portion, with the FRP reinforcement fully activated that is the challenge in the FRP reinforcement models. In the model by Matthys et al., the second linear portions of the curves for theoretical and experimental results mirror each other rather closely.

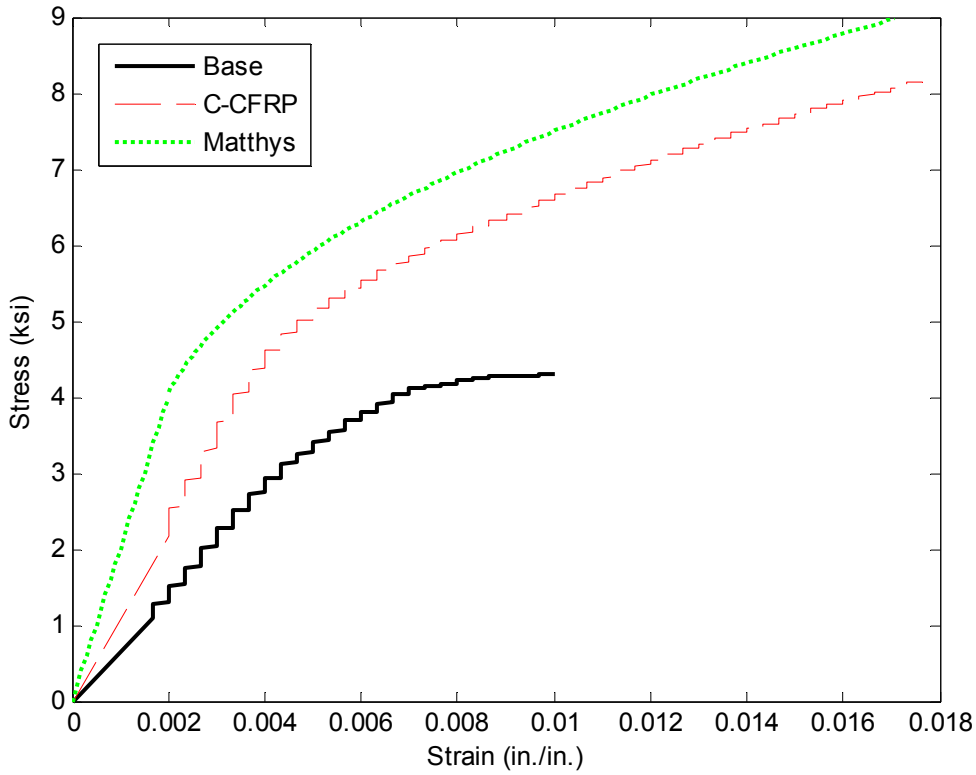

Figure 4.8 Theoretical Stress-Strain Plot of Carbon-FRP Sheets for Matthys et al.'s Model vs. Experimental Columns C-CFRP and Base

The model by Matthys et al. was further examined and compared with the C-FFRP-ST experimental column. Since this model was based off the earlier Toutanji model, it allowed for the use of equation 2.13, rather than 2.12 for the lateral elastic modulus and was therefore modeled separately. The resulting Figure 4.9 displays the resulting plot that resembles Figure 4.8. Figure 4.9 also has more deviation in the first region of the graph,

than in the second linear region. This is not a big problem and could be very easily corrected in the model since the FRP has not been activated in this region.

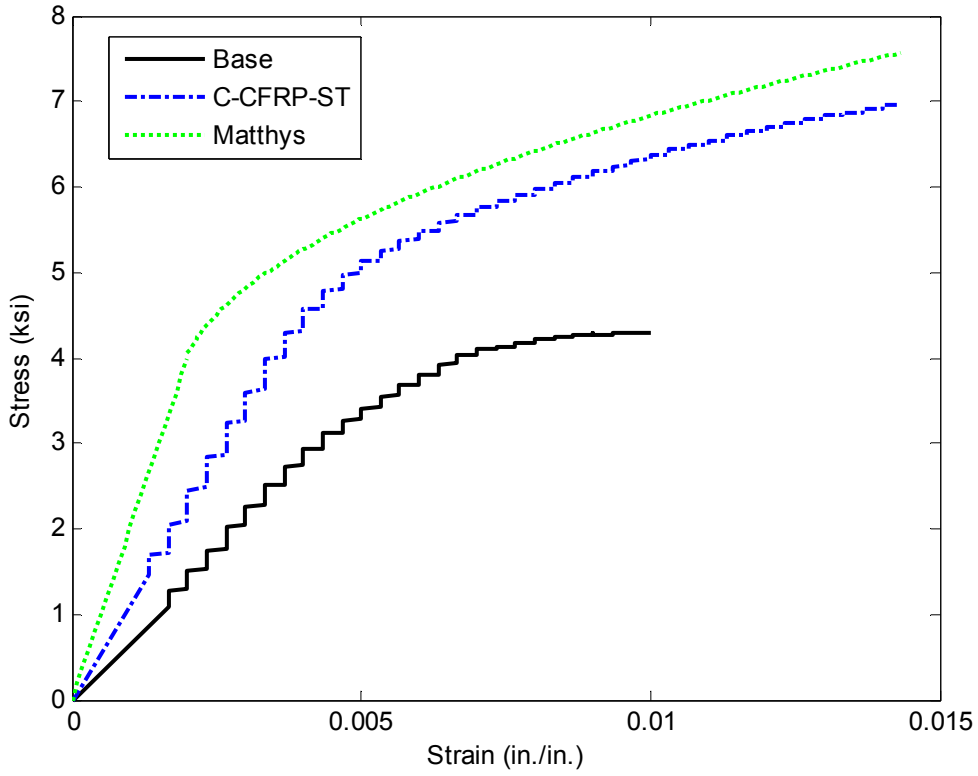

Figure 4.9 Theoretical Stress-Strain Plot of Carbon-FRP Strips for Matthys et al.'s Model vs. Experimental Columns C-CFRP-ST and Base

The least accurate result of all the Matthys et al. graphs is Figure 4.10 in which the Matthys et al. model is used for the experimental results of the C-GFRP column. Throughout this entire analysis, the C-GFRP column has provided the closest fitting curve to the theoretical. This is not true of the Matthys model. Figure 4.10 is the only model that under-estimates the stress and strain at the failure point of the curve. The model presented in Figure 4.10 actually does a good job of modeling the first linear

portion of the stress-strain curve, but it does not predict the strength of the FRP reinforcement with very much accuracy.

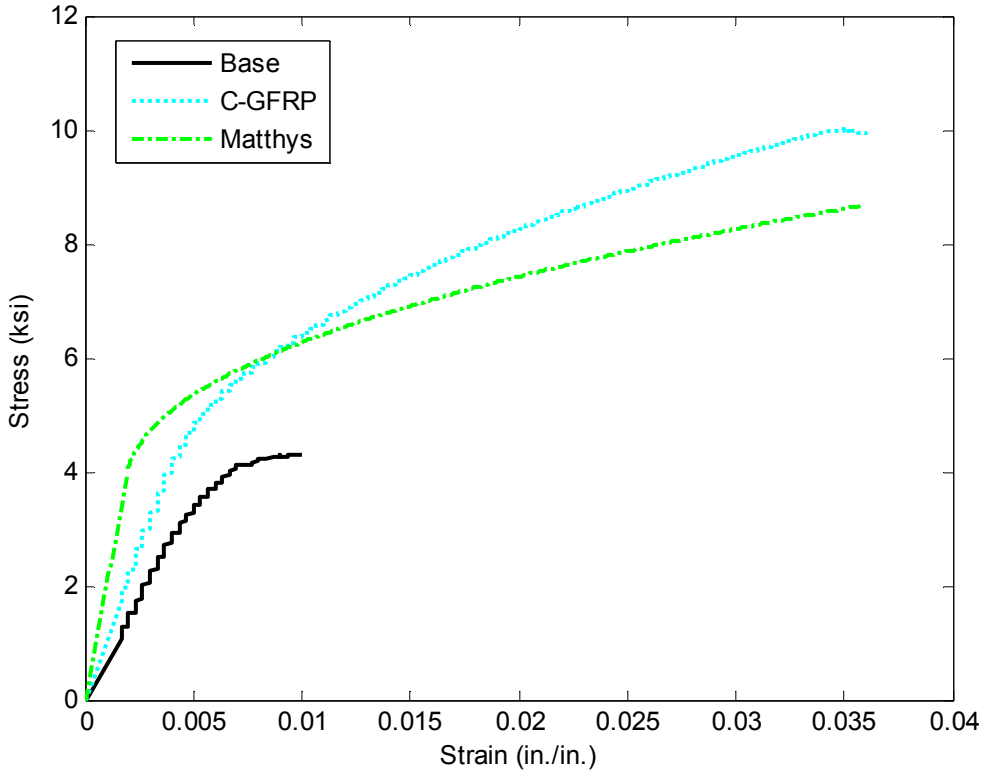

Figure 4.10 Theoretical Stress-Strain Plot of Glass-FRP Strips for Matthys et al.'s Model vs. Experimental Columns C-GFRP and Base

CHAPTER 5

CONCLUSIONS

5.1 Project Summary

Three recognized models in FRP reinforcement were analyzed and compared to experimental results found from the test on three columns retrofitted with FRP. The resulting stress-strain curves from the three experimental columns were plotted against the theoretical stress-strain curves proposed by the three models. Also, a “Base” column was analyzed to show the increase in strength provided by the FRP reinforcement. The “Base” column was modeled against a widely accepted reinforced concrete model by Mander et al. (1988) to determine the reliability of its results.

The research project was a continuation of a larger research project completed by Miller (2006) at The Ohio State University. The FRP reinforced columns were used for comparison in the project by Miller (2006), but are the focal point of this research project. The intent of this project is to see how the data that we have from that project for the load and concurrent displacement of the FRP reinforced columns matches up to the theoretical stress-strain curves of some popular models.

The resulting plots compared the theoretical and experimental models for all three test columns. They provide a good basis for the argument on whether the data may have some imperfections, or if the model may not be very strong for this type of application.

5.2 Summary of FRP Reinforcement Model Results

The intent of this project was to analyze FRP reinforcement models with a set of data that had not been examined in this area. The three models were analyzed, and there were some promising results. The model by Matthys et al. (2006) is the most accurate of the three models in predicting the experimental results. However, this is only true in the carbon-FRP column, as the glass-FRP column was not predicted accurately. The Toutanji (1999) and Samaan et al. (1998) models consistently over-estimated the strength of the columns.

Some problems existed in the FRP modeling results, but some of them can be easily explained. All 3 models had difficulty modeling the first linear portion of the bilinear stress-strain curve. However, this behavior is before the FRP is activated and therefore should not reflect poorly on the model. This inaccuracy was most likely to have been caused by the characteristics of the concrete being modeled incorrectly. For example, if an incorrect compressive stress is recorded for the concrete, the first linear curve could be slightly off of the results. This not only creates an incorrect modulus of elasticity, but an incorrect yield point at which the FRP reinforcement becomes activated. This point of activation is where the second linear curve begins, and the FRP reinforcement is activated.

Furthermore, it is believed that there might have been some problems with the application of the carbon-FRP reinforcement. This was especially noticeable in the Toutanji, and Matthys et al. models. The tensile modulus of the FRP reinforcement is included in the model, and it was reported in the specifications given by the SIKA® Corporation. However, the tensile modulus of the carbon-FRP was much higher than the glass-FRP. Yet, the glass-FRP reinforced column was stronger than either column with carbon strips or sheets. The higher tensile modulus in the carbon-FRP column should create a situation where more stress is required to reach a strain level as compared to the glass-FRP specimen with the smaller tensile modulus. The possible explanation for this is there might have been some problem in the application. If there was one weak spot in the carbon-FRP reinforcement, the entire column would fail because of it. This is a disadvantage of the FRP and may be relevant in this case.

Finally, a standardized experimental procedure is needed for testing FRP-reinforced columns. The over-estimation may have occurred because Toutanji (1999) used 2 wraps for one column, while Miller (2006) only wrapped the columns 1 ½ turns. There is no place in the model to correct for this change and this may have been a reason that the models over-estimated the strength of the experimental columns.

5.3 Further Study of FRP Reinforcement

This project on FRP reinforcement methods still has room for growth in the future. There are more models that were not used, and even more models that were not fully researched

due to time constraints. It would be a great service to this project to be able to model the data with all of the available models and then take the best one or two and attempt to improve upon them.

The future of FRP reinforcement as a viable alternative to traditional reinforcement methods is promising. This research project has shown that there are models that are very close to predicting the interaction of the FRP reinforced concrete columns. The key to the future of FRP reinforcement is more experimentation and more comparing and contrasting of existing models. Current papers by DeLorenzis and Tepfers, and Lam and Teng attempt to provide analysis of the varying models, and they provide some strong insight into these models. However, more experiments need to be completed because the only way to be sure in predicting the FRP reinforcement strength is to have solid results to support the model. The model must then support more data sets than its original data set that it was created to match. In closing, FRP reinforcement is a strong option in many cases of retrofitting and is likely to become a more popular alternative in the future.

LIST OF REFERENCES

Bischoff, C. R., ed. ACI Manual of Concrete Practice 2003. Farmington Hills, MI: 2003, 440R-1 – 440R-68.

Carreira D. J., & Chu K. (1985). Stress-Strain Relationship for Plain Concrete in Compression. *ACI Journal*, November-December 1985, 797-804.

Chaallal O., Hassan M., & LeBlanc, M. (2006). Circular Columns Confined with FRP: Experimental versus Predictions of Models and Guidelines. *Journal of Composites for Construction*, January/February 2006, 4-12.

De Lorenzis L., & Tepfers R. (2003). Comparative Study of Models on Confinement with Fiber-Reinforced Polymer Composites. *Journal of Composites for Construction*, August 2003, 219-237.

Fardis M. N., & Khalili, H. (1981). Concrete Encased in Fiberglass-Reinforced Plastic. *ACI Journal*, November-December 1981, 440-446.

Fardis M. N., & Khalili H. H. (1982). FRP-encased Concrete as a Structural Material. *Magazine of Concrete Research*, Vol. 34, No. 121: December 1982, 191-202.

Lam J., & Teng J.G. (2003). Design-Oriented Stress-Strain Model for FRP-Confined Concrete in Rectangular Columns. *Journal of Reinforced Plastics and Composites*, Vol. 22, No. 13, 2003, 1149-1186.

Lam J., & Teng J.G. (2002). Strength Models for Fiber-Reinforced Plastic-Confined Concrete. *Journal of Structural Engineering*, May 2002, 612-623.

Mander, J.B., Priestley, M.J.N., & Park, R. Theoretical Stress-Strain Model for Confined Concrete. *Journal of Structural Engineering,* December 1989, 1804-1825.

Miller, E. (2006). Experimental Research of Reinforced Concrete Column Retrofit Methods. Unpublished masters dissertation. The Ohio State University, Columbus.

Matthys, S., Toutanji, H., and Taerwe, L. (2006). Stress-Strain Behavior of Large-Scale Circular Columns Confined with FRP Composites. *Journal of Structural Engineering*, January 2006, 123-133.

Nystrom, Halvard E., Watkins, Steve E., Nanni, Antonio., Murray, Susan (2003). Financial Viability of Fiber-Reinforced Polymer (FRP) Bridges. *Journal of Management in Engineering*, January 2003, 2-8.

Pessiki, S., Harries K. A., Kestner J. T., Sause R., & Ricles, J. M. (2001). Axial Behavior of Reinforced Concrete Columns Confined with FRP Jackets. *Journal of Composites for Construction*, November 2001, 237-245.

Saadatmanesh, H., Ehsani, M.R., & Li, M.W. (1994). Strength and Ductility of Concrete Columns Externally Reinforced with Fiber Composite Straps. *ACI Structural Journal*, July-August 1994, 434-447.

Samaan M., Mirmiran A., & Shahawy M. (1998). Model of Concrete Confined by Fiber Composites. *Journal of Structural Engineering*, September 1998, 1025-1031.

Spiegel L., & Limbrunner G. F., (2003). *Reinforced Concrete Design. 5th ed*. New Jersey: Prentice Hall.

Spoelstra M. R., & Monti G. (1999). FRP-Confined Concrete Model. *Journal of Composites for Construction*, August 1999, 143-150.

Toutanji H. A. (1999). Stress-Strain Characteristics of Concrete Columns Externally Confined with Advanced Fiber Composite Sheets. *ACI Materials Journal*, May-June 1999, 397-404.

Appendix A

MATLAB Code for Examined Models

Mander et al. (1988)

```
>> %Stress-Strain of Confined and Unconfined Concrete:
>> %Mander et al. Model – Confined Concrete
>> %Area of longitudinal steel (Ast)
>> Ast=0.66; %(in^2)
>> %Area of concrete core (Acc in^2)
>> Acc=(pi/4)*5^2;
>> %Confined Concrete Ratio
>> pcc=Ast/Acc;
>> %s=transverse steel spacing
>> s=3; %in.
>> %ds=diameter of transverse reinforcement
>> ds=5; %in.
>> %ke=confinement effectiveness coefficient
>> ke=(1-s/(2*ds))/(1-pcc);
>> %ps=ratio of transvere steel to volume of confined concrete
>> %Asp=area of 1/4" dia. transverse wire
>> Asp=(pi/4)*(0.25)^2;
>> ps=(4*Asp)/(ds*s);
>> %fl=lateral confining stress
>> %fyh=transverse steel yield strength
>> fyh=57.898; %ksi
>> fl=(1/2)*ke*ps*fyh;
>> %fcc=confined concrete compressive strength
>> fco=4.149;
>> fcc=fco*(-1.254+2.254*sqrt(1+((7.94*fl)/fco))-2*fl/fco);
>> Ec=(57000*sqrt(4149))/1000; %ksi
>> eco=0.002;
>> %Confined Concrete Strains:
>> ecc=eco*(1+5*((fcc/fco)-1));
>> %Secant Modulus of Elasticity:
>> Esec=fcc/ecc;
>> r=Ec/(Ec-Esec);
>> ec=0:0.0001:0.03;
>> %Strain Ratio
>> x=ec./ecc;
>> %Axial Stress:
>> fc=(fcc.*x.*r)./(r-1+x.^r);
>> %Plot the Confined Reinforced Concrete Model
>> plot(ec,fc,'c:','LineWidth',2);
>> hold on
>> %Mander et al. Model – Unconfined Concrete
>> %Modulus of Elasticity:
>> Ec=(57000*sqrt(4149))/1000; %ksi
>> %Assumed failure strain:
>> ecou=0.002;
>> %Range of Strains to Failure:
>> ec1=0:0.0001:0.002;
>> %Maximum concrete compressive stress:
>> fcm=4.149; %ksi
```

```
>> %Secant Modulus for Unconfined Concrete:
>> Esecu=fcm./eco;
>> ru=Ec./(Ec-Esecu);
>> eccu=ecou*(1+5*(-1));
>> %Unconfined Concrete Strain Ratio
>> xu=ec1./ecou;
>> %Unconfined Concrete Stress
>> fcu=(fcm.*ru.*xu)./(ru-1+xu.^ru);
>> %Plot the unconfined concrete to failure:
>> plot(ec1,fcu, 'k','LineWidth',2 )
>> Develop straight line curve to spalling strain:
>> ec2=0.002:0.0001:0.006;
>> m=(-fcm/0.004);
>> y=m.*ec2 + fcm+2.0745;
>> plot(ec2,y,'k','LineWidth',2)
>> %Even matrices so the addition of fcc and fcu is possible:
>> ec3=0.006:0.0001:0.0298;
>> fcu3=ec3.*0;
>> plot(ec3,fcu3,'k','LineWidth',2)
>> %Define maximum and minimum values for axes:
>> axis ([0 0.03 0 6])
>> legend('Confined', 'Unconfined');
>> xlabel('Strain (in./in.) ','Fontsize',10);
>> ylabel('Stress (ksi)','Fontsize',10);
>> hold off
```

Load-Displacement Plot:

```
>> %Run the stress-strain plot above, then run this section so all the constants are recognized by MATLAB
>> %Area of cover Concrete:
>> Acover=(pi/4)*6^2-(pi/4)*5^2;
>> Acore=(pi/4)*5^2;
>> %Strains to be multiplied by the length
>> ecd=0:0.0001:0.03;
>> %Find the displacement:
>> delta=30.*ecd;
>> %Add the unconfined and confined compressive stresses:
>> fcutotal=[fcu,y,fcu3];
>> %Calculate the load, P
>> P=fc.*Acore+fcutotal.*Acover;
>> plot(delta,P,'c:','LineWidth',2);
>> hold on
>> %Load and Plot the base column
>> load N:\Research\RawData\BASEJa.txt;
>> B1=BASEJa(:,2);
>> B2=BASEJa(:,1);
>> plot(B1,B2,'k-','LineWidth',2);
>> legend('Mander et al.', 'Base');
>> xlabel('Displacement (in.)','Fontsize',10);
>> ylabel('Load (kips)','Fontsize',10);
>> hold off
```

Toutanji (1999)

Carbon Fiber-Reinforced Polymer:

Stress/Strain:

```
>> %Load Existing Load-Displacement Experimental Data:
>> %Base Column:
```

```
>> load N:\Research\RawData\BASEJas.txt;
>> B1=BASEJas(:,2)./30;
>> B2=BASEJas(:,1)./(pi*3^2);
>> %Plot the stress-strain curve:
>> plot(B1,B2,'k-','LineWidth',2);
>> hold on
>> %Carbon Sheets:
>> load N:\Research\RawData\C_CFRPJas.txt;
>> C1=C_CFRPJas(:,2)./30;
>> C2=C_CFRPJas(:,1)./(pi*3^2);
>> %Plot the stress-strain curve:
>> plot(C1,C2,'r--','LineWidth',2);
>> %Carbon Elastic Modulus:
>> Efc=234500;
>> %Carbon Sheet Thickness (m):
>> t=0.001016;
>> Radius of the Cylinder (m):
>> R=0.1524;
>> %Lateral Elastic Modulus:
>> Elc=Efc*t/R;
>> % Lateral Strain:
>> el=0:0.000001:0.0080;
>> %Lateral Stress:
>> fl=Elc.*el;
>> %Compressive Strength (MPA)
>> fc=28.6049;
>> %Axial Stress (MPA)
>> fa=fc.*(1+3.5.*(fl./fc).^0.85);
>> eo=0.002;
>> %Axial Strains (m/m)
>> ea=eo.*(1+(310.57.*el+1.90).*((fa/fc)-1));
>> %Convert MPA to ksi:
>> faus=fa.*0.1450377;
>> ea1=0:0.0001:0.002;
>> E=2100;
>> fa1=E.*ea1;
>> %Plot the second curve:
>> plot(ea1,fa1,'g-.','LineWidth',2)
>> %Plot the first curve:
>> plot(ea,faus,'g-.','LineWidth',2)
>> xlabel('Strain (in./in.)','Fontsize',10);
>> ylabel('Stress (ksi)','Fontsize',10);
>> legend('Base','C-CFRP','Toutanji');
>> hold off
```

Note: The Toutanji models for C-CFRP-ST and C-GFRP are similar with only small changes existing in material properties and a different equation for Lateral Elastic Modulus fot the Carbon Strips that was presented in Section 2.3.1.

Samaan et al. (1998)

Carbon Fiber-Reinforced Polymer:

Stress/Strain:

```
>> %Load and Plot the base column:
>> load N:\Research\RawData\BASEJas.txt;
>> B1=BASEJas(:,2)./30;
>> B2=BASEJas(:,1)./(pi*3^2);
>> plot(B1,B2,'k-','LineWidth',2);
```

```
>> hold on
>> %Load and Plot the Carbon Sheet Column Data:
>> load N:\Research\RawData\C_CFRPJas.txt;
>> C1=C_CFRPJas(:,2)./30;
>> C2=C_CFRPJas(:,1)./(pi*3^2);
>> plot(C1,C2,'r--','LineWidth',2);
>> %Load and Plot the Carbon Strips Column Data:
>> load N:\Research\RawData\C_CFRP_STJas.txt;
>> S1=C_CFRP_STJas(:,2)./30;
>> S2=C_CFRP_STJas(:,1)./(pi*3^2);
>> plot(S1,S2,'b-.','LineWidth',2);
>> %Samaan et. al. Model
>> %Carbon FRP
>> %Material Propoerties of Carbon FRP:
>> %Tensile Strength:
>> fj=123.2; %ksi
>> %Tensile Modulus:
>> Ej=10239.8; %ksi
>> %Thickness of the Carbon Wrap:
>> t=0.04; %in
>> %Diameter of Column:
>> D=6; %in
>> %Confinement Pressure:
>> frc=2*fj*t/D; %ksi
>> %Concrete Compressive Strength
>> fc=4149; %psi
>> %Intercept Stress:
>> foc=0.872*(fc/1000)+0.371*frc+0.908; %ksi
>> %First Secant Modulus
>> E1=47.586*sqrt(fc); %ksi
>> %Second Secant Modulus:
>> E2c=52.411*(fc/1000)+1.3456*(Ej*t/D); %ksi
>> %Range of Strains:
>> ec=0:0.0001:0.0175;
>> %Axial Stress:
>> fc=(((E1-E2c).*ec)./((1+(((E1-E2c).*ec)/foc).^1.5).^(1/1.5)))+E2c.*ec;
>> %Plot the Theoretical Stress-Strain Curve:
>> plot(ec,fc, 'g: ', 'LineWidth',2);
>> xlabel('Strain (in./in.)','Fontsize',10);
>> ylabel('Stress (ksi)','Fontsize',10);
>> legend('Base', 'C-CFRP','C-CFRP-ST','Samaan et. al.');
>> hold off
```

Note: The Samaan et al. models for C-GFRP are similar with only small changes existing in material properties.

Matthys et al. (2006)

Carbon-Fiber Reinforced Polymer:

Stress/Strain:

```
>> %Load Existing Load-Displacement Experimental Data:
>> %Base Column:
>> load N:\Research\RawData\BASEJas.txt;
>> B1=BASEJas(:,2)./30;
>> B2=BASEJas(:,1)./(pi*3^2);
>> %Plot the stress-strain curve:
>> plot(B1,B2,'k-','LineWidth',2);
>> hold on
```

```
>> %Carbon Sheets:
>> load N:\Research\RawData\C_CFRPJas.txt;
>> C1=C_CFRPJas(:,2)./30;
>> C2=C_CFRPJas(:,1)./(pi*3^2);
>> %Plot the stress-strain curve:
>> plot(C1,C2,'r--','LineWidth',1);
>> %Carbon Elastic Modulus:
>> Efc=234500;
>> %Carbon Sheet Thickness (m):
>> t=0.001016;
>> Radius of the Cylinder (m):
>> R=0.1524;
>> %Lateral Elastic Modulus:
>> Elc=Efc*t/R;
>> % Lateral Strain:
>> el=0:0.0001:0.014;
>> fl=Elc.*0.6.*el;
>> %Compressive Strength (MPA)
>> fc=28.06;
>> %Axial Stress (MPA)
>> fa=fc.*(1+2.3.*(fl./fc).^0.85);
>> eo=0.002;
>> %Axial Strains (m/m)
>> ea=eo.*(1+(310.57.*el+1.90).*((fa/fc)-1));
>> %Convert MPA to ksi:
>> faus=fa.*0.1450377;
>> ea1=0:0.0001:0.002;
>> E=2000;
>> fa1=E.*ea1;
>> %Plot the second curve:
>> plot(ea1,fa1,'g:','LineWidth',2)
>> %Plot the first curve:
>> plot(ea,faus,'g:','LineWidth',2)
>> xlabel('strain (in./in.)')
>> ylabel('stress (ksi)')
>> xlabel('strain (in./in.)','Fontsize',10);
>> ylabel('stress (ksi)','Fontsize',10);
>> xlabel('Strain (in./in.)','Fontsize',10);
>> ylabel('Stress (ksi)','Fontsize',10);
>> legend('Base','C-CFRP','Matthys');
>> hold off
```

Note: The Matthys et al. models for C-CFRP-ST and C-GFRP are similar with only small changes existing in material properties and a different equation for Lateral Elastic Modulus for the Carbon Strips that was presented in Section 2.3.1.